A cell-density dependent metabolic switch sensitizes breast cancer cells to ferroptosis

Elena Panzilius (1), Felix Holstein (1,5), Marie Bannier-Hélaouët (1,6), Christine von Toerne (2), Ann-Christine Koenig (2), Stefanie M. Hauck (2), Hilary M. Ganz (1), José P. Friedmann Angeli (3), Marcus Conrad (4) and Christina H. Scheel (1,7)

(1) Institute of Stem Cell Research, Helmholtz Center Munich, Neuherberg, Germany

(2) Research Unit Protein Science, Helmholtz Center Munich, Neuherberg, Germany

(3) Rudolf Virchow Center for Experimental Biomedicine, University of Würzburg, Würzburg, Germany

(4) Institute of Developmental Genetics, Helmholtz Center Munich, Germany

(5) Present address: Research Institute of Molecular Pathology (IMP), Vienna, Austria

(6) Present address: Hubrecht Institute, Utrecht, Netherlands

(7) Corresponding author: christina.scheel@helmholtz-muenchen.de

Running Title: Cell density regulates ferroptosis

Keywords: beta-oxidation/breast cancer/cell-density/ferroptosis/lipid droplets

Abstract

Ferroptosis is a regulated form of necrotic cell death caused by the accumulation of lipid peroxides. It can be induced by inhibiting glutathione peroxidase 4 (GPX4), the key enzyme for lipid peroxides reduction from phospholipid membranes. Recent studies have identified metabolic and genetic contributors to ferroptosis. However, many mechanisms of resistance or sensitivity to ferroptosis remain unknown. Here, we show that low cell density sensitizes primary mammary epithelial and breast cancer cells to induction of ferroptosis by GPX4 inhibition, whereas high cell density confers resistance. This effect occurs irrespective of oncogenic signaling or cellular phenotype and is not directly correlated to an increase in lipid peroxides. Mechanistically, we show that low cell density induces liberation of fatty acids from lipid droplets by adipose triglyceride lipase (ATGL) to fuel β-oxidation. Thereby, lipid-mediated toxicity is increased and exceeds a death-inducing threshold once GPX4 function is impaired. In conclusion, low cell-density regulated ferroptosis might serve as a mechanism to protect epithelial tissue integrity with the potential to be exploited in order to target disseminated breast cancer cells.

Introduction

A novel, regulated cell-death modality termed ferroptosis was recently described in specific cancer entities and other pathological settings [1,2]. Ferroptosis is caused by the accumulation of peroxidized lipids (lipoxygenation) and can be triggered by inhibition or genetic inactivation of glutathione peroxidase 4 (GPX4), the key enzyme in the removal of lipid hydroperoxides (L-OOH) from membrane phospholipids [2,3]. As its name indicates, ferroptosis is also dependent on intracellular iron, which is required for the accumulation of lipid hydroperoxides [1]. Moreover, cysteine availability affects glutathione (GSH) metabolism [4], and thus GPX4 activity and ferroptosis [1,2,5]. Apart from amino acid metabolism, lipid metabolism emerges as a determinant of ferroptosis sensitivity. In this context, the enzyme Acyl-CoA synthethase long chain family member 4 (ACSL4) has been shown to sensitize cells to ferroptosis by activating long-chain poly-unsaturated fatty acids (PUFAs) through formation of PUFA acyl-CoA (PUFA-CoA). PUFA-CoA are esterified into phosphatidylethanolamines (PE) which serve as a death signal for execution of ferroptosis [6,7]. However, despite these insights into molecular mechanisms, a better understanding of cellular and metabolic states that confer sensitivity or resistance to ferroptosis is crucial in order to exploit it for therapeutic purposes. These encompass triggering ferroptosis in cancer cells, as well as protecting cells from ferroptosis in other pathological conditions such as ischemia/reperfusion injury [8–10].

Here, we report that cell density induces a metabolic switch that sensitizes breast cancer cells to ferroptosis. Independently of cellular phenotype, oncogenic signaling and ACSL4 expression, we observe that high cell density confers resistance to ferroptosis triggered by pharmacological inhibition or genetic inactivation of GPX4. Mechanistically,

we show that low cell density triggers increased catabolism of neutral triglycerides from lipid droplets in order to channel fatty acids to mitochondria for β-oxidation. Indeed, blocking the release of triglycerides from lipid droplets restores resistance to GPX4-inhibition. Thus, we describe how cellular context can affect the metabolic state of breast epithelial and cancer cells, which in turn results in an increased sensitivity to ferroptosis.

Results and Discussion

Cell density sensitizes mammary epithelial cells to ferroptosis

Initially, we set out to assess whether immortalized human mammary epithelial cells (HMLE) were sensitive to induction of ferroptosis. We also included HMLE-Twist1 cells constitutively expressing the transcription factor Twist1 that, as a consequence, have undergone an Epithelial-Mesenchymal Transition (EMT). As described previously, HMLE cells display an epithelial morphology and express the epithelial marker E-cadherin, whereas Twist1-overexpression induces an EMT, resulting in downregulation of E-cadherin, expression of the mesenchymal marker Zeb1 and a mesenchymal morphology (Fig 1A and D) [11]. HMLE and HMLE-Twist1 cells were plated at three different cell densities ranging from sparse to sub-confluent and then treated with RSL3, an inhibitor of GPX4 (Fig 1A) [2]. We discovered that RSL3 induced cell death in a density-dependent manner: cells seeded at low density were highly sensitive while cells seeded at high density were resistant (Fig 1B and C). Moreover, cells plated at an intermediate cell density also showed moderate induction of cell death. We repeated these experiments using cells with a conditional Twist1- or Snail1-construct, another EMT-transcription factor [11–13]. Again, we observed density-dependent cell death upon RSL3-treatment in HMLE cells where Twist1 or Snail1 was induced for 15 days,

resulting in a full EMT (Fig EV1 A and B). As a control, an inactive diastereoisomer of RSL3 did not induce cell death at any cell density (Fig EV1A). Immunoblotting for GPX4 revealed that HMLE-Twist1 cells expressed 2.3-2.6 fold higher levels of GPX4 protein than HMLE cells. However, cell density itself did not have an effect on GPX4 protein expression (Fig 1D). Together, these data suggested that cell density is a critical factor sensitizing cells to GPX4 inhibition independent of whether HMLE cells were in an epithelial or mesenchymal state, thus contrasting with the recent finding that EMT predisposes cells to ferroptosis [14].

To confirm that ferroptosis was indeed the observed modality of cell death, we treated cells at low seeding density with zVAD-fmk (zVAD), thereby blocking caspase activity [15], and Nec1-S, an inhibitor of the receptor-interacting protein kinase 1 (RIPK1) [16]. We also used Ferrostatin1 (Fer1) and Liproxstatin1 (Lip1) as known inhibitors of ferroptosis [1,9]. Indeed, we observed that RSL3-induced cell death was only rescued by treatment with Fer1 or Lip1, but not zVAD or Nec1-S, suggesting that neither apoptosis nor necrosis, respectively, are involved (Fig 1E, EV1C). In addition, immunoblotting showed no cleavage of caspase 3 or its downstream target PARP upon RSL3-treatment in both HMLE and HMLE-Twist1 cells, further ruling out apoptosis as a cell-death modality (Fig 1F) [17,18].

To confirm that ferroptosis-induction at low cell density was exclusively dependent on GPX4-inhibition and not related to off-target effects or simply overall change in the ratio of inhibitor molecules and cell number, we knocked out *GPX4*. Using CRISPR/Cas9, we derived several single cell clones (SCCs) with and without detectable GPX4 protein expression (*GPX4*-WT and *GPX4*-KO, respectively, Fig 1G). Since gene knockout of *GPX4* was previously shown to be lethal [19,20], SCCs were kept in Lip1-containing

growth medium. In addition, treatment with Fer1 maintained viability as well (Fig EV1D). Upon withdrawal of Lip1, we again observed induction of cell death only at a low cell density in three *GPX4*-KO SCCs of both HMLE and HMLE-Twist1 cells (Fig 1H) similar to what was reported for Tamoxifen-inducible *GPX4* knockout fibroblasts [3]. Importantly, SCCs with intact GPX4 expression still showed density-dependent cell death upon RSL3 treatment, suggesting that selected SCCs are representative of the respective bulk population (Fig EV1E and F). In conclusion, we observed that cell-density determines sensitivity to ferroptosis in both epithelial and Twist1-expressing mesenchymal HMLE cells.

Cell-density dependent cell death is not affected by oncogenic signaling and occurs in primary mammary epithelial cells

Next, we addressed whether oncogenic signaling affects density-dependent sensitivity to ferroptosis. However, both HMLE cells overexpressing HRas or neuNT oncogenes and HMLE-Twist1 cells overexpressing HRas remained resistant to RSL3-induced cell death at high seeding densities and died at low cell densities, similar to their parental cells (Fig 2A and EV2A). In addition, we tested whether deletion of the tumor suppressor *PTEN* altered sensitivity to RSL3-treatment, but again, we did not see an effect beyond cell density (Figure 2B and EV2B). In conclusion, neither oncogenic signaling nor an epithelial or a mesenchymal cell state impacted cell-density dependent cell death. Interestingly, investigation of an association between the mutation status of RAS and ferroptosis sensitivity in 117 cancer cell lines did not reveal a selective lethality [21], further supporting the notion that still poorly understood and reversible, non-mutational mechanisms regulate ferroptosis-sensitivity.

To determine whether cell-density dependent ferroptosis-sensitivity constitutes an intrinsic property of mammary epithelial cells, primary human mammary epithelial cells (HMECs) isolated from three different donors (M1, M2 and M3) were treated with RSL3 (Fig 2C). In addition, we included prospectively isolated primary cells of the basal lineage to dissect whether lineage identity had an effect on sensitivity to ferroptosis induction (Fig EV2C) [22][12]. Again, we observed density-dependent cell death by RSL3 to a similar extent in all samples. Importantly, this effect occurred both in ambient oxygen atmosphere (20%) as well as 3% oxygen, the latter mimicking physiological tissue pressure (Fig 2C and EV2C). Together, these data indicate that cell-density dependent sensitivity to ferroptosis is a trait present in primary HMECs and does not arise as an artefact of long-term culture and selection.

GPX4-inhibition prevents organoid-generation in 3D-collagen gels

Next, we wished to determine whether density-dependent sensitivity to ferroptosis could be observed when cells are grown in a 3D-environment, thus mimicking a physiological environment. For this purpose, we plated primary HMEC into an organoid assay as previously described [22]. Specifically, bulk primary HMEC as well as prospectively isolated cells of the basal (B, $CD10^{+}/CD49f^{hi}/EpCAM^{-}$) and luminal progenitor lineage (L, $CD10^{-}/CD49f^{+}/EpCAM^{+}$) were plated into 3D-collagen gels. After initial establishment of cultures from single cells and before the onset of organoid formation, RSL3, Lip1 or a combination of both were added to the growth medium every 2-3 days. In the DMSO control and Lip1-treated cells, basal cells gave rise to branched organoids and luminal cells formed spheres, while bulk cells gave rise to different kind of colonies including branched organoids and spheres (Fig 2D and EV2D), as reported previously [22]. RSL3-

treatment strongly inhibited colony formation, an effect that was partially rescued by concomitant treatment with Lip1 (60-100% of control, Fig 2D and EV2D). In addition, in contrast to control and rescued samples, we observed a complete absence of proliferation marker Ki67 in the few remaining small clusters of cells in RSL3-treated cultures (Fig 2E). Together, these data suggested that primary HMEC are highly sensitive to GPX4-inhibition during organoid formation from single cells.

To provide further support for these observations, HMLE *GPX4*-KO SCCs were seeded at different densities in 3D-collagen gels in medium with (+Lip1) or without Lip1 (−Lip1) or cultured for three days in Lip1-containing medium with subsequent Lip1-withdrawal (+/−Lip1, Fig 2F). This allowed us to test whether cells remain sensitive to ferroptosis once small colonies have formed. As previously described in HMLE cells, *GPX4*-KO SCCs generated multicellular spheres in Lip1-containing medium (Fig EV2E) [12]. Similar to low seeding densities in 2D-cultures, immediate withdrawal of Lip1 in 3D-cultures resulted in complete growth-inhibition (Fig 2F and EV2E). In contrast, Lip1-withdrawal after three days of 3D-culture enabled colony-formation in similar numbers compared to culture in Lip1-containing growth medium. These data indicated that once colonies have formed, they acquire resistance to cell death induction by *GPX4* knockout. However, both colony-size as well as proliferation assessed by Ki67 staining were reduced in this condition, suggesting that Lip1-withdrawal at later timepoints restricts further expansion in 3D-cultures (Fig 2F and G). Together, these data indicate that, similar to low seeding densities in 2D-culture, both primary HMEC as well as HMLE cells are sensitive to ferroptosis at low cell-density in 3D-culture. However, the observation that HMLE *GPX4*-KO SCCs were partially protected from ferroptosis upon Lip1-withdrawal once small colonies had formed, suggests an intrinsic mechanism that

protects epithelial tissues from ferroptosis. In line with these data, a recent study showed that in immortalized non-tumorigenic MCF10A cells and a panel of breast cancer cell lines, detachment of cells from the extracellular matrix (ECM) triggers ferroptosis [23]. Further, it was shown that Tamoxifen-inducible *GPX4*-knockout fibroblasts are capable of tumor formation when implanted subcutaneously in mice at very high numbers (5 million) [24].

Cell density-dependent death induced by GPX4-inhibition is dependent on iron and lipoxygenation, but independent of ACSL4

Ferroptosis has been linked to the levels of poly-unsaturated fatty acids (PUFAs) in cellular membranes, which are particularly prone to oxygenation (Fig 3A) [6,7,25]. Therefore, in order to further characterize cell-density dependent ferroptosis, we undertook a series of experiments modulating PUFA-incorporation and -oxygenation. Recent studies showed that ACSL4, which plays a key role in lipid biosynthesis and fatty acid degradation, is an essential enzyme for ferroptosis execution [6,7]. ACSL4 increases the PUFA-content within phospholipids, which are susceptible to oxidation. In turn, lipoxygenases (LOX) generate oxygenated phospholipids that serve as a death signal for ferroptosis unless they are reduced by GPX4. Consequently, blocking ACSL4 activity by rosiglitazone (ROSI) or LOX activity by PD146176 or BWA4C was shown to protect against ferroptosis [6,9,25]. Lip1, Fer1, or the lipophilic antioxidant α-tocopherol (α-toc) can also prevent accumulation of lipid oxygenation and thus, execution of ferroptosis. Moreover, since the labile iron pool (redox-active Fe^{2+}) contributes to lipid oxygenation via the Fenton reaction, chelation of iron by deferoxamine (DFO) or cyclopirox (CPX) protects against ferroptosis (Fig 3A) [1].

To understand why cells die in a cell-density dependent manner, we tested the ability of the aforementioned inhibitors to rescue RSL3-induced cell death. Thus, we observed that iron-chelation by DFO, but not CPX, partially rescued RSL3-induced cell death in both HMLE and HMLE-Twist1 cells (28% to 72% viability in HMLE and 17% to 55% viability in HMLE-Twist1 cells upon DFO-co-treatment, Figure 3B). In contrast to DFO, CPX directly chelates iron intracellularly and thereby affects iron-containing enzymes as well [26], suggesting that excessive iron chelation might produce opposing effects. Inhibition of lipoxygenases by both PD146176 and BWA4C, as well as the antioxidant α-toc, rescued RSL3-induced cell death (Fig 3B). Together, these results suggested that oxygenated PUFA-containing lipids contribute to density-dependent cell death (Fig 3B), in line with recent studies showing that LOX enzymes oxidize PUFAs, thereby sensitizing them to ferroptosis [9,25]. To assess whether ACSL4 contributes to the intracellular PUFA-containing lipid pool, cells were pre-treated with ROSI prior to treatment with RSL3 to allow changes in the lipid profile to occur. Surprisingly, ROSI treatment did not rescue cell-death induction in HMLE and HMLE-Twist1 cells upon RSL3-treatment (Fig 3B). Importantly, none of the employed inhibitors showed cytotoxic effects on HMLE and HMLE-Twist1 when applied alone (Fig 3B). ROSI is an agonist of the peroxisome proliferation-activated receptor-γ (PPAR-γ), and ACSL4 inhibition is only an off-target effect [27]. Therefore, to validate whether ACSL4 contributes to density-dependent cell death, we performed a CRISPR/Cas9-mediated *ACSL4* knockout in HMLE *GPX4*-KO SCCs (Fig 3C, 1G and 1H). We derived several clones with *ACSL4* knockout (*ACSL4*-KO: A1, A3, A4, A5, A7 and A8) and control clones with intact ACSL4 expression (A2 and A6 respectively, Fig 3C). Unexpectedly, all clones died irrespective of ACSL4 expression in a cell-density dependent manner upon withdrawal of Lip1 (Fig

3C, lower panel), suggesting that ferroptosis occurred independently of ACSL4. Of note, we cannot rule out that another ACSL enzyme compensated for ACSL4 activity, since ACSL3 can use PUFAs as a substrate as well [28,29].

To determine whether levels of oxidized lipids correlated with ferroptosis sensitivity, we measured lipid-derived reactive oxygen species (ROS) levels using the fluorescent dye BODIPY 581/591 C11 [30]. Consistently with previous observations [1,9,21], we noticed an increase in C11 fluorescence in *GPX4* knockout cells upon Lip1-withdrawal in both HMLE and HMLE-Twist1 cells at all densities (Fig 3D and E). However, this increase in C11 greatly varied between different SCCs (Fig 3D), although all of them were similarly sensitized to ferroptosis at low seeding densities (Fig 1H). On average, C11 fluorescence increased at least 2-fold upon Lip1-withdrawal in HMLE *GPX4*-KO SCCs irrespective of seeding density (Fig 3E). Interestingly, HMLE-Twist1 *GPX4*-KO SCCs seeded at an intermediate density showed the strongest accumulation of C11 fluorescence (5-fold on average, Fig 3E). In summary, Lip1-withdrawal led to an increase in lipid-derived ROS levels in HMLE and HMLE-Twist1 *GPX4*-KO SCCs in all seeding densities. Therefore, the observed increase in lipoxygenation did not correlate with induction of ferroptosis. Consequently, these data suggest that cells at high and low seeding densities cope differently with an increase in lipid-derived ROS levels, rather than cell density having a strong impact on overall levels of lipoxygenation.

Proteomics reveal a density-dependent metabolic switch that sensitizes cells to ACSL4-independent ferroptosis

Given the observed disconnection between lipoxygenation levels and cell death induced by inhibition or loss of GPX4, we next assessed why HMLE and HMLE-Twist1 cells

plated at high cell density were resistant to ferroptotic cell death whereas cells plated at low cell density were sensitive. To do so, a proteomic study was performed to assess which proteins were differentially expressed at high and low cell densities alone and upon GPX4-inhibition through RSL3-treatment (Fig 4A). For data analysis, we focused on upregulated proteins, by at least 1.5-fold in low cell density compared to high cell density in both HMLE and HMLE-Twist1 cells (190 proteins, $p<0.05$). Further, we selected proteins that were upregulated at least 1.5-fold upon RSL3-treatment in both cell lines compared to non-RSL3 treated controls (274 proteins, $p<0.05$). Furthermore, we assessed the upregulated overlapping proteins (119 proteins) between low cell density and RSL3 treatment, with the rationale that these proteins are potentially involved in cell-density dependent death. The obtained list of 119 proteins was submitted to GO-term enrichment analysis (biological processes) using DAVID (Fig 4A and EV3A) [31,32]. The GO-term “positive regulation of triglyceride catabolic process” within the top-ten regulated pathways attracted our attention, since GPX4 is crucial for removal of lipid peroxides within phospholipid membranes (Fig 4A and EV3A).

Within this list, we decided to focus on adipose triglyceride lipase (ATGL = *PNPLA2*), which is the initial enzyme for triacylglyceride (TAG) hydrolysis and is regulated by its co-activator ABHD5 [33]. Functionally, ATGL catalyzes TAGs from intracellular lipid droplets (LDs), reducing LD abundance [34]. We validated ATGL expression by immunoblotting and observed an upregulation of ATGL in both HMLE and HMLE-Twist1 cells at low compared to high seeding densities (Fig 4B). Next, we stained neutral TAGs with the fluorescent dye BODIPY493/503 which is commonly used to assess the content of lipid droplets within cells [34]. Thereby, we observed a positive correlation between BODIPY493/503 fluorescence and seeding density in both HMLE and HMLE-Twist1

cells (Fig 4C). Cells at high density showed a higher fluorescence intensity which decreased in lower seeding densities (Fig 4C), indicating that cells at low density have a lower lipid-droplet content compared to cells at higher density. In contrast, we observed the opposite effect when we stained for basal lipid ROS by C11-BODIPY. Both HMLE and HMLE-Twist1 cells showed an elevation of lipid ROS levels from high to low seeding densities (Fig 4C). Next, we inhibited ATGL by pre-incubating both HMLE and HMLE-Twist1 cells with the ATGL inhibitor Atglistatin (ATG) prior GPX4-inhibition by RSL3 at low density. RSL3-induced cell death was rescued by simultaneous ATG treatment in both HMLE and HMLE-Twist1 cells without affecting viability in control treatments (Fig 4D). Moreover, ATGL inhibition by ATG also rescued cell death induced by Lip1-withdrawal in *GPX4*-KO SCCs H5 and HT1 (Fig EV3B). Together, these data suggested that cell density regulates ATGL expression in order to liberate fatty acids from TAGs stored in LDs. This in turn increased lipid-mediated stress in cells at low density, inducing a vulnerability towards simultaneous GPX4 inhibition.

Several reports suggest that in well-fed cells fatty acids are stored as TAGs within LDs and that starvation or cellular stress lead to a release of fatty acids from LDs by cytoplasmic lipases such as ATGL. These fatty acids are then transferred to mitochondria for oxidative metabolism [35–37]. Thus, we aimed to determine whether the upregulation of ATGL-mediated LD degradation served to satisfy changing metabolic needs at low cell density. Indeed, we observed that enzymes required for β-oxidation such as the Carnitine Palmitoyltransferase 1A (CPT1A) or the Acetyl-CoA Acyltransferase 2 (ACAA2) were upregulated at low compared to high density in the proteomic data set in both HMLE and HMLE-Twist1 cells (Supplemental Table 1). By RT-qPCR, we verified density-dependent regulation of both CPT1A and ACAA2 in each

cell line (Fig 4E and EV3C). We then measured basal mitochondrial ROS levels by MitoSox staining and detected an increase in MitoSox fluorescence in a density-dependent manner, suggesting an increased production of mitochondrial ROS at low density, possibly due to an increased rate of β-oxidation (Fig 4F). To examine this further, we treated HMLE and HMLE-Twist1 cells with Etomoxir (ETX) to inhibit CPT1A, the rate-limiting enzyme for β-oxidation. However, ETX-treatment alone decreased cell viability in both HMLE and HMLE-Twist1 cells (Fig 4G), suggesting that β-oxidation generally serves as an important energy source in these cells. Of note, a combination of ETX and RSL3 treatment had only minor effects on cell death induction at low cell density compared to treatment with each drug alone (Fig 4G). Moreover, in *GPX4*-KO SCCs HT1 and H5, ETX treatment alone reduced viability compared to controls in all densities (Fig EV3D). However, cells at the lowest cell density were around 1.5-fold less viable than cells in the highest density, suggesting an increased sensitivity to inhibition of β-oxidation at low cell density (Fig EV3D). Upon Lip1- withdrawal and thus *GPX4* knockout, we did not observe strong additive effects upon ETX-treatment (Fig EV3D). Thus, HMLE and HMLE-Twist1 cells appear to rely heavily on β-oxidation, with cells at low density being further sensitized to its inhibition. Together our data suggest that cell density regulates ATGL-mediated LD degradation in order to fuel β-oxidation at low density.

Stimulating β-oxidation through catabolism of LDs could be relevant to drive breast cancer metastasis, especially during stages where cells are disseminated as single cells or small clusters [37–39]. Thus, a metabolic switch to increased β-oxidation induced by cell density appears to occur at the expense of inducing a vulnerability towards lipid peroxidation. Based on these considerations, we asked whether increasing the LD

amount by other means than ATGL inhibition could likewise decrease lipid-mediated stress and thus lower toxicity of GPX4-inhibition at low cell density. Previous studies have shown that culturing cells with the mono-unsaturated fatty acid oleic acid (OA) increases the lipid droplet content within cells [34]. Based on these considerations, we fed HMLE and HMLE-Twist1 cells with 100 µM OA for 24h and assessed LD content by BODIPY493/503 staining. For both cell lines, we observed an increase in LD content upon OA treatment in all densities compared to control (Fig 4H, left panel). Interestingly, feeding OA to cells also decreased lipid ROS levels compared to controls (Fig 4H, right panel), indicating a negative correlation between lipid droplet amount and ROS levels. We then assessed viability upon GPX4 inhibition by RSL3 of control and OA-treated HMLE and HMLE-Twist1 cells. OA completely rescued RSL3-induced cell death induced at low and intermediate seeding densities (Fig 4I), whereas OA treatment alone only had a minor impact on cell viability (Fig EV3E). Together, these data suggest that culturing cells with OA protects them from lipid-stress induced by liberation of fatty acids from LDs, thereby providing a possible explanation for the beneficial effect of OA in rescuing RSL3-induced ferroptosis that has already been reported in other cancer cell lines [25].

Based on these considerations, we hypothesized that ATGL-mediated TAG degradation, required for β-oxidation, might lead to toxic accumulation of lipid ROS upon GPX4 inhibition through peroxidation of these liberated fatty acids. This mechanism appears to be independent of ACSL4 expression that increases oxidation-prone PUFAs in membranes as *ACSL4* knockout did not rescue ferroptotic cell death at low density (Fig 3F) [6,7]. Moreover, we did not observe a direct correlation between overall lipid ROS levels and cell death upon *GPX4*-knockout (Fig 1, Fig 3C and D). In line with these observations, it was recently reported that every measure leading to a reduction of

autoxidizable lipids, particularly PUFAs, will inhibit ferroptosis [40]. Thus, influencing LD content and turnover by changing the fraction of less oxidation-prone fatty acids such as OA might buffer lipotoxic effects, as was recently proposed [37,41]. Supporting our findings, it was previously determined that cells at high density have an increased cell-to-cell heterogeneity in lipid droplet content, which was suggested to reduce lipotoxicity for the whole population [42].

In summary, we have shown that cell density plays a critical role in determining sensitivity to ferroptosis in both primary mammary epithelial and breast cancer cells. This sensitivity is associated with cell-density dependent regulation of lipid droplets and thus liberation of fatty acids, serving as a source for β-oxidation. Future studies will be needed to determine whether this metabolic switch serves to protect epithelial tissue integrity. Given the recognition that, at least for melanoma, cellular antioxidant potential is required for efficient metastasis [43], this mechanism might provide a strategy to target breast cancer cells during stages of metastasis, where they are present as single or small clusters of cells, for example following systemic dissemination into distant tissues.

Materials and Methods

Chemicals

The following chemicals were purchased from Sigma: Atglistatin, α-tocopherol, Bovine serum albumin (BSA), BW4AC, Ciclopriox, Deferoxamine, Dimethyl sulfoxide (DMSO), Doxorubicine hydrochloride, Etomoxir, Ferrostatin-1, Liproxstatin-1, Necrostatin-1S, Oleic Acid-Albumin from bovine serum, PD146176, Rosiglitazone. RSL3 was purchased from Cayman Chemical. z-VAD-fmk was purchased from R&D Systems.

Cell lines

Primary mammary epithelial cells were isolated and cultured as previously described [22]**.** Immortalized HMLE cells were generated by retroviral transduction of SV40 large T early region and catalytic subunit of human telomerase enzyme (hTERT) [44]. HMLE-Twist1 were subsequently generated by transduction with a pBabe-Puro-Twist1 vector, leading to constitutive Twist1-overexpression and a mesenchymal phenotype [45]. HMLE-Ras cells were generated by introduction of a pBabe-Puro-Ras (V12H) retroviral vector [44] and HMLE-neu-NT cells with a pWZL-vector containing a mutated form of the HER2/neu oncogene [11]. Cells were grown in a 37°C incubator with a humidified atmosphere of 5% CO_2, except for primary cells, which were maintained at 3% oxygen level if not otherwise stated. All cells were cultured in mammary epithelial cell growth medium containing 0.004 ml/ml BPE, 10 ng/ml EGF, 5 µg/ml Insulin and 0.5 µg/ml hydrocortisone (PromoCell) supplemented with 1% Pen/Strep (Invitrogen) (MECGM). For *GPX4*-knockout single cell clones of HMLE and HMLE-Twists1 cells (for generation see CRISPR/Cas9-mediated knockout of individual genes section), 500 nM to 1 µM Lip1 was additionally added to MECGM. Inducible HMLE-Twist1-ER cells and HMLE-Snail1-

ER cells were generated as described and cultured in presence of 10 µg/ml blasticidin (Life Technologies) [11]. For induction of EMT, cells were additionally treated with 20 nM 4-hydroxy-tamoxifen (TAM, Sigma) for the indicated number of days.

To visualize cell death induced by RSL3, HMLE and HMLE-Twist1 cells were plated in 6-well plates at a density of 90000 (high), 30000 (med) and 10000 (low) cells, corresponding to 3000 (high), 1000 (med) and 333 (low) seeded cells per well of 96-wells plates. The next day, cells were treated with 0.1% DMSO or 100 nM RSL3 and 20-24h later, bright-field images were taken on a Leica DM IL LED microscope.

Viability Assays

To measure the viability of cells in different densities, cells were seeded in 96-wells plates at a density of 3000, 1000 and 333 cells per well (high, med and low respectively, 3-6 technical replicates). Treatment with DMSO control or RSL3 was started one day after plating and cells were treated for 20-24h. For rescue-experiments (Fig 1E and 3B), cells were seeded at a density of 600 cells per well. Compounds employed in viability assays were added during RSL3 treatment, except for Rosiglitazone, Oleic acid and Atglistatin (additionally 24-48h pre-treatment). For assessment of the viability of CRISPR/Cas9 *GPX4*-knockout clones and *GPX4*/*ACSL4*-knockout clones, Lip1 was withdrawn from the medium directly on the day of plating. For all experiments, viability was measured 48h after plating using CellTiter-Glo assay (Promega). CellTiter-Glo assay is a luciferase-based assay that measures endogenous ATP levels that correlate with the number of metabolically active, and thus viable cells. Luminescence was detected using the Luminometer Centro XS^3 LB 960 (Berthold Technologies). Obtained RLU values were averaged and normalized to respective DMSO control or Lip1 control.

Immunoblotting

For blotting against GPX4, 1.5 x 10^6 and 0.3 x 10^6 cells (high and low) cells were seeded on 15-cm dishes corresponding to 3000 and 600 cells per wells of 96-wells plates. For ATGL protein detection, 516000, 172000 and 57000 cells (high, med and low) were seeded in 10-cm dishes, corresponding to 3000, 1000 and 333 cells in 96-wells. For detection of apoptosis markers, cells were seeded at a density of 500000 cells in 15-cm dishes corresponding to 1000 cells (med) in 96-wells, treated the next day for 20h with 0.1% DMSO, 100 nM RSL3 or 10 µM Doxorubicin. For pAKT and total AKT assessment, seeding density in 10-cm dishes corresponded to 3000 cells in 96-well and for starvation of cells, medium was changed on the second day to basal DMEM/F12 overnight. For all experiments, protein isolation was performed 48h after plating. Briefly, dishes were washed with PBS, cells scraped off on ice, pelleted and resuspended in RIPA buffer (50 mM Tris pH 8.0, 150 mM NaCl, 1% NP-40, 0.5% sodium deoxycholate, 0.1% sodium dodecyl sulfate and 5 mM EDTA pH 8.0) containing phosphatase and protease inhibitor cocktails (Sigma). Protein concentration was measured using the DC Protein Assay (Bio-Rad Laboratories). Protein lysates (10-20 µg) were separated on 12.5% SDS-PAGE gels followed by wet-blot transfer to PVDF membranes. Western blotting was performed using the following primary antibodies: GPX4 (EPNCIR144, ab125066, Abcam, 1:2000), ACSL4 (A5, sc-271800, Santa Cruz, 1:100), E-cadherin (EP700Y, GTX61329, Biozol, 1:25000), Zeb1 (HPA027524, Sigma, 1:5000), phospho-Akt Ser473 (D9E, 4060, Cell Signaling Technology, 1:2000), pan Akt (C67E7, 4691, Cell Signaling Technology, 1:1000), Caspase 3 (9662, Cell Signaling Technology, 1:1000), cleaved Caspase 3 Asp175 (5A1E, 9664, Cell Signaling Technolgy, 1:1000), PARP

(9542, Cell Signalling Technology, 1:1000) or ATGL (2138, Cell Signaling Technology, 1:1000). beta-actin (AC-15, ab6276, Abcam, 1:6000) was used as loading control. Afterwards, membranes were incubated with appropriate horseradish peroxidase-linked secondary antibodies (111-036-045 and 115-036-062, Jackson ImmunoResearch, 1:12500) followed by detection of chemiluminescence with ECL Prime Western Blotting Detection Reagent (GEHealthcare) on a ChemiDoc Imaging System using Image Lab software (Bio-Rad Laboratories). ImageJ software was used for densitometric analysis of protein bands.

Flow cytometric assessment of lipid peroxidation, neutral triglyceride content and mitochondrial ROS level

200000, 66000 and 22000 cells (high, med and low) were seeded in 6-cm dishes which corresponds to 3000, 1000 and 333 cells in 96-wells. Ferroptosis in GPX4 knockout clones was induced by direct withdrawal of Lip1 from the culture medium and lipid peroxidation was measured the next day. To assess basal lipid peroxidation, mitochondrial reactive oxygen species (ROS) or neutral triglyceride content (=Lipid Droplet (LD) content) in density, measurements using respective dyes were performed 48h after plating. Treatment with Oleic Acid was conducted for 24h prior to measurement. For lipid peroxidation assessment and mitochondrial ROS level, cells were stained with 2 µM BODIPY-C11 581/591 (ThermoFisher) or 5 µM MitoSox (ThermoFisher) for 30 min at 37°C and to assess the neutral triglyceride/LD content, cells were stained with 2 µM BODIPY493/503 (ThermoFisher) for 15 min at 37°C. Cells were washed with PBS, harvested by trypsinization and resuspended in PBS containing 1% BSA for flow cytometric analysis. 1 µM Sytox blue staining (ThermoFisher) was used

to discriminate live/dead cells. At least 10000 cells per sample were immediately recorded on a FACS Aria IIIu (BD Biosciences) using laser and filters according to manufacturer's instructions of the respective dye. Data was analyzed using FlowJo Software (FlowJo, LLC).

RNA preparation and RT-qPCR Analysis

For density experiments, 200000, 66000 and 22000 cells (high, med and low) were seeded in 6-cm dishes which corresponds to 3000, 1000 and 333 cells in 96-wells. Two days after plating, mRNA was isolated using the RNeasy Mini Kit (Qiagen) according to manufacturer's instructions. 1 µg total RNA was reverse transcribed using Oligo(dT) primers for amplification (OneScript cDNA Kit, abm). For qPCR, specific primers were used in a power SYBR Green-PCR Master Mix reaction (Applied Biosystems) which was run in a Quantstudio 12K Flex qPCR System (Applied Biosystems). *RPL32* was used for normalization. The following primer sequences were used:

RPL32: forward 5'-CAGGGTTCGTAGAAGATTCAAGGG-3' and reverse 5'-CTTGGAGGAAACATTGTGAGCGATC-3', *CPT1A*: forward 5'-ATCAATCGGACTCTGGAAACGG-3' and reverse 5'- TCAGGGAGTAGCGCATGGT-3', *ACAA2*: forward 5'-CTGCTCCGAGGTGTGTTTGTA-3' and reverse 5'-GGCAGCAAATTCAGACAAGTCA-3'

CRISPR/Cas9-mediated knockout of individual genes

Benchling software as well as the MIT CRISPR design tool (http://crispr.mit.edu/) were used to design sgRNA guides for targeting critical exons of GPX4, ACSL4 and PTEN. For GPX4 and ACSL4 knockout, string assembly gRNA cloning (STAgR) was employed

to clone sgRNAs into the STAgR_Neo plasmid as recently described [46]. For Gibson Assembly reaction, a Gibson Assembly Master Mix (NEB) was used according to manufacturer's instructions and diluted 1:4 prior transformation into XL10-Gold ultracompetent cells (Agilent Technologies). For GPX4 and ACSL4 gene knockout, the CRISPR/Cas9 system was transiently expressed. Briefly, 150000 to 200000 cells were seeded in 6-well dishes and cultured for 24h. Cells were then co-transfected using TransIT-X2 transfection reagent (Mirus Bio LLC) at a ratio 1:3 (approximately 1 µg each) of a Cas9-GFP-expressing plasmid (pSpCas9(BB)-2A-GFP) and respective STAgR-Neo plasmid containing sgRNAs according to manufacturer's instructions. 72h after transfection, cells were sorted for GFP expression on a FACSAriaIIIu (BD Biosciences), Single cells were seeded into 96-wells and expanded. To assess CRISPR/Cas9-induced deletions or insertions, PCRs of the expected corresponding genomic locus were performed and validated by sequencing and immunoblotting of the respective proteins.

The following sgRNA sequences were used: GPX4: 5'-TTTCCGCCAAGGACATCGAC-3', 5'-CGTGTGCATCGTCACCAACG-3' and 5'-ACTCAGCGTATCGGGCGTGC-3', ACSL4: 5'-ATTGTTATTAACAAGTGGAC-3', 5'-CTAGCTGTAATAGACATCCC-3' and 5'-TGCAATCATCCATTCGGCCC-3'.

For PTEN deletion, sgRNA was cloned into a pLX-sgRNA vector (Addgene plasmid#50662) [47]. HMLE-Twist1-ER 24hi cells were stably transduced with lentiviruses expressing a doxycycline-inducible Cas9 protein (pCW-Cas9, Addgene #50661) [47] and selected with 1 µg/ml puromycin (Sigma). Then, cells were stably transduced with lentiviruses containing the sgRNAs against PTEN. In these cells, Cas9 expression was activated with 0.5 µg/ml doxycycline treatment (Sigma) to allow CRISPR/Cas9-mediated modification in the PTEN locus and single cells were seeded in

96-well plates. Clones were screened by performing PCR and sequencing of the expected corresponding genomic locus. Successful PTEN deletion was validated by assessing activation status of downstream AKT signaling by immunoblotting. The following sgRNA sequence was used to target PTEN: 5'-TGTGCATATTTATTACATCG-3'

Culture in 3D collagen gels, carmine staining of gels and 3D immunofluorescence

3D collagen gels (final concentration 1.3 mg/ml collagen I) were prepared and cultured as previously described [22]. For HMLE SCC H5 *GPX4* knockout, 675, 225 and 75 cells (high, med and low) per 24-well gel were seeded in 500 nM Lip1 containing medium or directly withdrawn of Lip1. After 3 days, all gels were washed with PBS and for the +/− Lip1 condition, Lip1 was removed by changing the culture medium. For primary mammary epithelial cell culture, 5000 cells were seeded per 24-well gel. After 5 days of initial survival culture in mammary epithelial cell growth medium (MECGM, Promocell) containing 3 µM Y-27632 (Biomol), 10 µM Forskolin (Adipogen) and 0.5% FCS (PAN Biotech), MECGM medium was supplemented with a final concentration of 0.1% DMSO, 100 nM RSL3, 500 nM Lip1, or the combination of 100 nM RSL3 and 500 nM Lip1. Medium was replaced every 2 days and gels were fixed with 4% paraformaldehyde (PFA, Sigma) after 7-11 days of culture. Carmine staining and imaging was performed as previously described [22]. Pictures were analyzed by ImageJ software. For this purpose, images were first converted to a binary image and colonies extracted from the background by setting a manual threshold. Particles with an area between 400 and 90000 μm^2 (20-300 µM diameter) and a circularity 0.5-1 were counted. 3D immunofluorescence was performed as previously described [22]. Primary antibodies

used were: Vimentin (V9, MAB3578, Abnova, 1:100) and Ki67 (ab15580, Abcam, 1:300). Following secondary antibodies used were: Donkey anti-Rabbit IgG Alexa Fluor 546 (A10040, Thermo Fisher, 1:250), Donkey anti-Mouse IgG Alexa Fluor 488 (A21202, Thermo Fisher, 1:250). Pictures were taken on an Olympus Confocal (20x magnification) using FV10-ASW software.

Proteomic analysis of cells seeded in cell density

516000, 172000 and 57000 cells (high, med and low) were seeded on 10-cm dishes, corresponding to 3000, 1000 and 333 cells in 96-wells. For RSL3 treatment, cells at intermediate density were treated the next day for 5h with 100 nM RSL3 prior isolation of proteins. Proteins of cells were isolated 48h after seeding. Protein isolation and concentration measurement was performed as described in immunoblotting section.

MS sample preparation

10 µg of sample were enzymatically digested using a modified filter-aided sample preparation (FASP) protocol [48,49]. Peptides were stored at -20°C until MS measurement.

MS measurement

Mass spectrometry (MS) measurements were performed in data dependent (DDA) mode. MS data were acquired on a Q Exactive (QE) high field (HF) mass spectrometer (Thermo Fisher Scientific Inc.). Approximately 0.5 µg per sample were automatically loaded to the online coupled RSLC (Ultimate 3000, Thermo Fisher Scientific Inc.) HPLC system. A nano trap column was used (300 µm inner diameter (ID) × 5 mm, packed with Acclaim PepMap100 C18, 5 µm, 100 Å; LC Packings, Sunnyvale, CA) before separation by reversed phase chromatography (Acquity UPLC M-Class HSS T3 Column 75µm ID x

250mm, 1.8µm; Waters, Eschborn, Germany) at 40°C. Peptides were eluted from column at 250 nl/min using increasing acetonitrile (ACN) concentration (in 0.1% formic acid) from 3% to 41 % over a 105 minutes gradient. The high-resolution (60 000 full width at half-maximum) MS spectrum was acquired with a mass range from 300 to 1500 m/z with automatic gain control target set to 3×10^6 and a maximum of 50 ms injection time. From the MS prescan, the 10 most abundant peptide ions were selected for fragmentation (MSMS) if at least doubly charged, with a dynamic exclusion of 30 seconds. MSMS spectra were recorded at 15 000 resolution with automatic gain control target set to 1×10^5 and a maximum of 100 ms injection time. Normalized collision energy was set to 28 and all spectra were recorded in profile type.

Progenesis QI for label-free quantification

Spectra were analyzed using Progenesis QI software for proteomics (Version 3.0, Nonlinear Dynamics, Waters, Newcastle upon Tyne, U.K.) for label-free quantification as previously described [49] with the following changes: spectra were searched against the Swissprot human database (Release 2017.02, 553473 sequences). Search parameters used were 10 ppm peptide mass tolerance and 20 mmu fragment mass tolerance. Carbamidomethylation of cysteine was set as fixed modification and oxidation of methionine and deamidation of asparagine and glutamine was allowed as variable modifications, allowing only one missed cleavage site. Mascot integrated decoy database search was set to a false discovery rate (FDR) of 1 %.

Analysis of proteomic study

Proteins were filtered for a regulation of at least 1.5-fold in RSL3 treatment compared to non-RSL3 treated control and a regulation of at least 1.5-fold in the lowest cell density compared to the highest cell density for both HMLE and HMLE-Twist1 cells. Only

proteins with a p-value below 0.05 (unpaired, two-tailed T-test with Welch's correction on log2 expression data) were submitted to GO term enrichment analysis using DAVID [31,32]. Potential hits were further analyzed by functional assays.

Data presentation and statistical analyses

Data are presented as mean ± SEM of n = x experiments, with x indicating the number of independent experiments performed, unless stated otherwise. Statistical analysis was performed using GraphPad Prism 7.0 software or Excel 2016. In general, an unpaired, two-tailed T-test was performed with Welch's correction and a p-value below 0.05 was considered significant.

Authors contributions

E.P. and C.H.S. conceived the study and designed experiments. E.P., F.H., M.B.-H. and H.M.G. performed *in vitro* experiments and analyzed data. C.v.T., A-C.K. and S.M.H. performed proteomics and analyzed the data. J.P.F.A. and M.C. provided reagents and participated in discussion, evaluation and interpretation of the data. E.P. assembled the figures. E.P. and C.H.S. interpreted the data and wrote the manuscript. All authors read and approved the final manuscript.

Acknowledgements

We thank Christopher Breunig and Stefan Stricker (Institute of Stem Cell Research, Helmholtz Zentrum Munich) for sharing reagents and guidance for STAgR cloning. We thank members of the Scheel Group, especially Lisa Meixner and Laura Eichelberger, for sharing experimental expertise. Further, we thank Thomas Schwarz-Romond, Alecia-

Jane Twigger, Massimo Saini and Laura Eichelberger for critical reading of the manuscript, Magdalena Götz, Andreas Jung and all members of the Scheel group for productive discussion of the data. E.P. was supported by a Boehringer Ingelheim Fonds PhD fellowship. This work was supported by a grant of the German Cancer Aid Foundation (Max Eder Program, Deutsche Krebshilfe 110225) to C.H.S., and grants by the German Federal Ministry of Education and Research (BMBF) through the Joint Project Modelling ALS Disease In Vitro (MAIV, 01EK1611B) and the VIP + program NEUROPROTEKT (03VP04260) to M.C.

Conflict of interest

The authors declare no conflict of interest.

References

1. Dixon SJ, Lemberg KM, Lamprecht MR, Skouta R, Zaitsev EM, Gleason CE, Patel DN, Bauer AJ, Cantley AM, Yang WS, et al. (2012) Ferroptosis: an iron-dependent form of nonapoptotic cell death. *Cell* **149**: 1060–1072.
2. Yang WS, SriRamaratnam R, Welsch ME, Shimada K, Skouta R, Viswanathan VS, Cheah JH, Clemons PA, Shamji AF, Clish CB (2014) Regulation of ferroptotic cancer cell death by GPX4. *Cell* **156**: 317–331.
3. Seiler A, Schneider M, Förster H, Roth S, Wirth EK, Culmsee C, Plesnila N, Kremmer E, Rådmark O, Wurst W, et al. (2008) Glutathione peroxidase 4 senses and translates oxidative stress into 12/15-lipoxygenase dependent- and AIF-mediated cell death. *Cell Metab* **8**: 237–248.
4. Ishii T, Sugita Y, Bannai S (1987) Regulation of glutathione levels in mouse

spleen lymphocytes by transport of cysteine. *J Cell Physiol* **133**: 330–336.

5. Hayano M, Yang WS, Corn CK, Pagano NC, Stockwell BR (2016) Loss of cysteinyl-tRNA synthetase (CARS) induces the transsulfuration pathway and inhibits ferroptosis induced by cystine deprivation. *Cell Death Differ* **23**: 270–278.
6. Doll S, Proneth B, Tyurina YY, Panzilius E, Kobayashi S, Ingold I, Irmler M, Beckers J, Aichler M, Walch A, et al. (2017) ACSL4 dictates ferroptosis sensitivity by shaping cellular lipid composition. *Nat Chem Biol* **13**: 91–98.
7. Kagan VE, Mao G, Qu F, Angeli JPF, Doll S, Croix CS, Dar HH, Liu B, Tyurin VA, Ritov VB, et al. (2017) Oxidized arachidonic and adrenic PEs navigate cells to ferroptosis. *Nat Chem Biol* **13**: 81–90.
8. Linkermann A, Skouta R, Himmerkus N, Mulay SR, Dewitz C, De Zen F, Prokai A, Zuchtriegel G, Krombach F, Welz P-S, et al. (2014) Synchronized renal tubular cell death involves ferroptosis. *Proc Natl Acad Sci* **111**: 16836–16841.
9. Friedmann Angeli JP, Schneider M, Proneth B, Tyurina YY, Tyurin V a, Hammond VJ, Herbach N, Aichler M, Walch A, Eggenhofer E, et al. (2014) Inactivation of the ferroptosis regulator Gpx4 triggers acute renal failure in mice. *Nat Cell Biol* **16**: 1180–1191.
10. Gao M, Monian P, Quadri N, Ramasamy R, Jiang X (2015) Glutaminolysis and Transferrin Regulate Ferroptosis. *Mol Cell* **59**: 298–308.
11. Mani S a, Guo W, Liao M-J, Eaton EN, Ayyanan A, Zhou AY, Brooks M, Reinhard F, Zhang CC, Shipitsin M, et al. (2008) The epithelial-mesenchymal transition generates cells with properties of stem cells. *Cell* **133**: 704–715.
12. Schmidt JM, Panzilius E, Bartsch HS, Irmler M, Beckers J, Kari V, Linnemann JR, Dragoi D, Hirschi B, Kloos UJ, et al. (2015) Stem-Cell-like Properties and

Epithelial Plasticity Arise as Stable Traits after Transient Twist1 Activation. *Cell Rep* **10**: 131–139.

13. Casas E, Kim J, Bendesky A, Ohno-Machado L, Wolfe CJ, Yang J (2011) Snail2 is an essential mediator of twist1-induced epithelial mesenchymal transition and metastasis. *Cancer Res* **71**: 245–254.
14. Viswanathan VS, Ryan MJ, Dhruv HD, Gill S, Eichhoff OM, Seashore-Ludlow B, Kaffenberger SD, Eaton JK, Shimada K, Aguirre AJ, et al. (2017) Dependency of a therapy-resistant state of cancer cells on a lipid peroxidase pathway. *Nature* **547**: 453–457.
15. SLEE EA, ZHU H, CHOW SC, MacFARLANE M, NICHOLSON DW, COHEN GM (1996) Benzyloxycarbonyl-Val-Ala-Asp (OMe) fluoromethylketone (Z-VAD.FMK) inhibits apoptosis by blocking the processing of CPP32. *Biochem J* **315**: 21–24.
16. Degterev A, Huang Z, Boyce M, Li Y, Jagtap P, Mizushima N, Cuny GD, Mitchison TJ, Moskowitz MA, Yuan J (2005) Chemical inhibitor of nonapoptotic cell death with therapeutic potential for ischemic brain injury. *Nat Chem Biol* **1**: 112–119.
17. Boulares a H, Yakovlev AG, Ivanova V, Stoica B a, Wang G, Iyer S, Smulson M, Chem MJB (1999) Role of Poly (ADP-ribose) Polymerase (PARP) Cleavage in Apoptosis. *J Biol Chem* **274**: 22932–22940.
18. Wolf BB, Schuler M, Echeverri F, Green DR (1999) Caspase-3 is the primary activator of apoptotic DNA fragmentation via DNA fragmentation factor-45/inhibitor of caspase-activated DNase inactivation. *J Biol Chem* **274**: 30651–30656.
19. Imai H, Hirao F, Sakamoto T, Sekine K, Mizukura Y, Saito M, Kitamoto T, Hayasaka M, Hanaoka K, Nakagawa Y (2003) Early embryonic lethality caused by targeted disruption of the mouse PHGPx gene. *Biochem Biophys Res Commun*

305: 278–286.

20. Yant LJ, Ran Q, Rao L, Van Remmen H, Shibatani T, Belter JG, Motta L, Richardson A, Prolla TA (2003) The selenoprotein GPX4 is essential for mouse development and protects from radiation and oxidative damage insults. *Free Radic Biol Med* **34**: 496–502.
21. Yang WS, SriRamaratnam R, Welsch ME, Shimada K, Skouta R, Viswanathan VS, Cheah JH, Clemons P a, Shamji AF, Clish CB, et al. (2014) Regulation of ferroptotic cancer cell death by GPX4. *Cell* **156**: 317–331.
22. Linnemann JR, Miura H, Meixner LK, Irmler M, Kloos UJ, Hirschi B, Bartsch HS, Sass S, Beckers J, Theis FJ, et al. (2015) Quantification of regenerative potential in primary human mammary epithelial cells. *Development* **142**: 3239–3251.
23. Brown CW, Amante JJ, Goel HL, Mercurio AM (2017) The α6β4 integrin promotes resistance to ferroptosis. *J Cell Biol* **216**: 4287–4297.
24. Schneider M, Wortmann M, Mandal PK, Arpornchayanon W, Jannasch K, Alves F, Strieth S, Conrad M, Beck H (2010) Absence of Glutathione Peroxidase 4 Affects Tumor Angiogenesis through Increased 12/15-Lipoxygenase Activity. *Neoplasia* **12**: 254–263.
25. Yang WS, Kim KJ, Gaschler MM, Patel M, Shchepinov MS, Stockwell BR (2016) Peroxidation of polyunsaturated fatty acids by lipoxygenases drives ferroptosis. *Proc Natl Acad Sci* **113**: E4966–E4975.
26. Cao JY, Dixon SJ (2016) Mechanisms of ferroptosis. *Cell Mol Life Sci* **73**: 2195–2209.
27. Kim JH, Lewin TM, Coleman RA (2001) Expression and characterization of recombinant rat acyl-CoA synthetases 1, 4, and 5: Selective inhibition by triacsin

C and thiazolidinediones. *J Biol Chem* **276**: 24667–24673.

28. Van Horn CG, Caviglia JM, Li LO, Wang S, Granger DA, Coleman RA (2005) Characterization of recombinant long-chain rat Acyl-CoA synthetase isoforms 3 and 6: Identification of a novel variant of isoform 6. *Biochemistry* **44**: 1635–1642.
29. Ansari IH, Longacre MJ, Stoker SW, Kendrick MA, O'Neill LM, Zitur LJ, Fernandez LA, Ntambi JM, MacDonald MJ (2017) Characterization of Acyl-CoA synthetase isoforms in pancreatic beta cells: Gene silencing shows participation of ACSL3 and ACSL4 in insulin secretion. *Arch Biochem Biophys* **618**: 32–43.
30. Drummen GPC, Van Liebergen LCM, Op den Kamp JAF, Post JA (2002) C11-BODIPY581/591, an oxidation-sensitive fluorescent lipid peroxidation probe: (Micro)spectroscopic characterization and validation of methodology. *Free Radic Biol Med* **33**: 473–490.
31. Huang DW, Sherman BT, Lempicki RA (2009) Systematic and integrative analysis of large gene lists using DAVID bioinformatics resources. *Nat Protoc* **4**: 44–57.
32. Huang DW, Sherman BT, Lempicki RA (2009) Bioinformatics enrichment tools: Paths toward the comprehensive functional analysis of large gene lists. *Nucleic Acids Res* **37**: 1–13.
33. Wang H, Bell M, Sreenevasan U, Hu H, Liu J, Dalen K, Londos C, Yamaguchi T, Rizzo MA, Coleman R, et al. (2011) Unique regulation of adipose triglyceride lipase (ATGL) by perilipin 5, a lipid droplet-associated protein. *J Biol Chem* **286**: 15707–15715.
34. Smirnova E, Goldberg EB, Makarova KS, Lin L, Brown WJ, Jackson CL (2006) ATGL has a key role in lipid droplet/adiposome degradation in mammalian cells. *EMBO Rep* **7**: 106–113.

35. Rambold AS, Cohen S, Lippincott-Schwartz J (2015) Fatty acid trafficking in starved cells: Regulation by lipid droplet lipolysis, autophagy, and mitochondrial fusion dynamics. *Dev Cell* **32**: 678–692.

36. Wright HJ, Hou J, Xu B, Cortez M, Potma EO, Tromberg BJ, Razorenova O V. (2017) CDCP1 drives triple-negative breast cancer metastasis through reduction of lipid-droplet abundance and stimulation of fatty acid oxidation. *Proc Natl Acad Sci* **114**: E6556–E6565.

37. Jarc E, Kump A, Malavašič P, Eichmann TO, Zimmermann R, Petan T (2018) Lipid droplets induced by secreted phospholipase A2and unsaturated fatty acids protect breast cancer cells from nutrient and lipotoxic stress. *Biochim Biophys Acta - Mol Cell Biol Lipids* **1863**: 247–265.

38. Park JH, Vithayathil S, Kumar S, Sung PL, Dobrolecki LE, Putluri V, Bhat VB, Bhowmik SK, Gupta V, Arora K, et al. (2016) Fatty Acid Oxidation-Driven Src Links Mitochondrial Energy Reprogramming and Oncogenic Properties in Triple-Negative Breast Cancer. *Cell Rep* **14**: 2154–2165.

39. Camarda R, Zhou AY, Kohnz RA, Balakrishnan S, Mahieu C, Anderton B, Eyob H, Kajimura S, Tward A, Krings G, et al. (2016) Inhibition of fatty acid oxidation as a therapy for MYC-overexpressing triple-negative breast cancer. *Nat Med* **22**: 427–432.

40. Shah R, Shchepinov MS, Pratt DA (2018) Resolving the Role of Lipoxygenases in the Initiation and Execution of Ferroptosis. *ACS Cent Sci* **4**: 387–396.

41. Nguyen TB, Louie SM, Daniele JR, Tran Q, Dillin A, Zoncu R, Nomura DK, Olzmann JA (2017) DGAT1-Dependent Lipid Droplet Biogenesis Protects Mitochondrial Function during Starvation-Induced Autophagy. *Dev Cell* **42**: 9–

21.e5.

42. Herms A, Bosch M, Ariotti N, Reddy BJN, Fajardo A, Fernández-Vidal A, Alvarez-Guaita A, Fernández-Rojo MA, Rentero C, Tebar F, et al. (2013) Cell-to-cell heterogeneity in lipid droplets suggests a mechanism to reduce lipotoxicity. *Curr Biol* **23**: 1489–1496.

43. Piskounova E, Agathocleous M, Murphy MM, Hu Z, Huddlestun SE, Zhao Z, Leitch AM, Johnson TM, DeBerardinis RJ, Morrison SJ (2015) Oxidative stress inhibits distant metastasis by human melanoma cells. *Nature* **527**: 186–191.

44. Elenbaas B, Spirio L, Koerner F, Fleming MD, Zimonjic DB, Donaher JL, Popescu NC, Hahn WC, Weinberg RA (2001) Human breast cancer cells generated by oncogenic transformation of primary mammary epithelial cells. *Genes Dev* **15**: 50–65.

45. Yang J, Mani SA, Donaher JL, Ramaswamy S, Itzykson RA, Come C, Savagner P, Gitelman I, Richardson A, Weinberg RA, et al. (2004) Twist , a Master Regulator of Morphogenesis , Plays an Essential Role in Tumor Metastasis Ben Gurion University of the Negev. *Cell* **117**: 927–939.

46. Breunig CT, Durovic T, Neuner AM, Baumann V, Wiesbeck MF, Köferle A, Götz M, Ninkovic J, Stricker SH (2018) One step generation of customizable gRNA vectors for multiplex CRISPR approaches through string assembly gRNA cloning (STAgR). *PLoS One* **13**: 1–12.

47. Wang T (2014) Genetic Screens in Human Cells Using. **80**: 80–85.

48. Wiśniewski JR, Zougman A, Nagaraj N, Mann M (2009) Universal sample preparation method for proteome analysis. *Nat Methods* **6**: 359–362.

49. Grosche A, Hauser A, Lepper MF, Mayo R, von Toerne C, Merl-Pham J, Hauck

SM (2016) The Proteome of Native Adult Müller Glial Cells From Murine Retina.

Mol Cell Proteomics **15**: 462–480.

Figure Legends

Figure 1: Cell density sensitizes mammary epithelial cells to ferroptosis

A. Bright-field microscopy: HMLE and HMLE-Twist1 cells were seeded at three different densities for 24h, then treated with 0.1% DMSO or 100 nM RSL3 for 24h prior imaging. Scale bar: 200 µm
B. Viability assay: treatment of HMLE and HMLE-Twist1 (HTwist1) with 100 nM RSL3 in cell density, n=6
C. Dose-response curves: treatment of HMLE (H) and HMLE-Twist1 (HT) seeded at indicated densities with 3-fold dilutions of RSL3, n=4
D. Immunoblot: E-cadherin (E-Cad), GPX4, Zeb1 and beta-actin protein expression in HMLE and HMLE-Twist1 (HTwist1) cells at high (hi) and low density. Upper beta-actin serves as loading control for E-cad and GPX4, lower beta-actin for Zeb1. Numbers indicate densitometric ratios of detected GPX4 protein to beta-actin band in percent. kDa = kilo Dalton
E. Rescue-viability assay: treatment of HMLE and HMLE-Twist1 cells with DMSO control, 500 nM Ferrostatin (Fer1), 500 nM Liproxstatin1 (Lip1), 10 µM Necrostatin (Nec1-S), 50 µM zVAD-fmk (zVAD) or 100 nM RSL3 alone or in a combination with RSL3 at low density, mean of at least three biological replicates (n=3-5)
F. Immunoblot: protein expression of cleaved and total PARP, cleaved Caspase 3 and Caspase 3 (Casp3) and beta-actin in HMLE and HMLE-Twist1 cells upon DMSO, 100 nM RSL3 or 10 µM Doxorubicin (DOX) treatment at intermediate density. Doxorubicin serves as positive control for PARP and Casp3 cleavage. beta-actin serves as loading control. From top to bottom, numbers indicate densitometric ratios

of detected protein PARP, cleaved PARP, Casp3 and cleaved Casp3 to beta-actin band in percent. kDa = kilo Dalton. n.d. = not detectable.

G. Immunoblot: GPX4 and beta-actin protein expression in Single Cell Clones (SCCs) upon CRISPR/Cas9-mediated modification in the *GPX4* locus and parental bulk HMLE and HMLE-Twist1 cells. beta-actin serves as loading control. kDa = kilo Dalton.

H. Viability assay: Lip1 withdrawal of SCCs with *GPX4*-KO seeded at the indicated density, related to Fig 1G, n=2 for HMLE and n=4 for HMLE-Twist1 SCCs

Data are presented as mean of indicated biological replicates ± SEM (n=x). Viability was normalized to respective DMSO control (B, D, E) or to respective Lip1 control (H) within each seeding density and cell line. Statistics: two-tailed, unpaired T-test with Welch's correction (p-value: *<0.05, **<0.01, ***0.001, ****<0.0001, n.s. = not significant).

Fig EV1

A. Viability assay: treatment of epithelial (–TAM) or 15 days 4-hydroxytamoxifen-induced mesenchymal (15d+TAM) HMLE-Twist1-ER 24^{high} cells with 0.3% DMSO control, 300 nM RSL3 or 300 nM of an inactive isomer of RSL3 in density, n=3

B. Viability assay: treatment of epithelial (–TAM) or 15 days 4-hydroxytamoxifen-induced mesenchymal (15d+TAM) HMLE-Snail1-ER 24^{high} cells with 0.3% DMSO control or 300 nM RSL3, n=1

C. Rescue-viability assay: control treatment HMLE and HMLE-Twist1 cells with DMSO, 500 nM Ferrostatin1 (Fer1), 500 nM Liproxstatin1 (Lip1), 10 µM Necrostatin1-S (Nec1-S) or 50 µM zVAD-fmk (zVAD) at low density, mean of at least three biological replicates (n=3-5), related to Fig 1E

D. Viability assay: CRISPR/Cas9-derived HMLE Single Cell Clones (SCCs) of HMLE and HMLE-Twist1 upon 1 µM Lip1, Lip1 withdrawal or 500 nM Fer1 at density, n=2 for HMLE SCCs and n=3-4 for HMLE-Twist1 SCCs, related to Fig1G and H
E. Viability assay of CRISPR/Cas9-derived control HMLE Clones (SCCs) with wildtype (WT) GPX4 expression upon 1 µM Lip1 (control), 100 nM RSL3 or deprivation of Lip1 at density, n=2, related to Fig 1G
F. Viability assay of CRISPR/Cas9-derived HMLE-Twist1 Single Cell Clones (SCCs) as described in E, n=2-4, related to Fig 1G

Data are presented as mean of indicated biological replicates ± SEM (n=x). Data was normalized to respective DMSO control (A,B,C) or to respective Lip1 control (D-F) within each seeding density and cell line. Statistics: two-tailed, unpaired T-test with Welch's correction (p-value: *<0.05, **<0.01, ***0.001, ****<0.0001, n.s. = not significant).

Figure 2: Cell-density dependent cell death is maintained during cellular transformation and prevents growth in 3D-collagen gels

A. Viability assay: treatment of HMLE, HMLE-HRas (G12V), HMLE-neuNT with 0.3% DMSO or 300 nM RSL3 cells in density, n=2
B. Viability assay: treatment of *PTEN*-wildtype (WT) and two *PTEN*-knockout clones (KO-1 and KO-2) of HMLE-Twist1-ER cells (without Twist1-activation) in density, n=3
C. Viability assay: treatment of bulk primary mammary epithelial cells of three different Donors (M1, M2, M3) with 0.1% DMSO or 100 nM RSL3 at ambient oxygen level (20%) or oxygen levels present in tissues (normoxia, 3%) in density, n=3
D. 3D-collagen gels: Sorted CD10-positive basal (B) or luminal progenitor (L) primary mammary epithelial cells were treated with 0.1% DMSO, 100 nM RSL3, 500 nM Lip1

or a combination of RSL3 and Lip1 for 7-10d prior quantification of arising colonies. Bright-field images of representative colonies and the mean of 3-4 technical replicates ± s.d. of one representative experiment from two independent experiments performed are shown. Scale: 200 µm.

E. Confocal microscopy of 3D-collagen gels: staining of colonies quantified in Figure 2D with Ki67 (red), vimentin (green) or DAPI (blue, nuclear staining).

F. 3D-collagen gels: HMLE single cell clone H5 with *GPX4*-knockout (KO) was seeded at different densities in 3D collagen gels in medium containing 500 nM Lip1 (+Lip1), withdrawn of Lip1 either directly (-Lip1) or after 3d in initial +Lip1 culture (+/- Lip1) for 7-10 days. Mean of 3-4 technical replicates ± s.d. of one representative experiment from two independent experiments performed are shown.

G. Confocal microscopy of 3D-collagen gels: staining of colonies derived from the intermediate density with Ki67 (red), vimentin (green) or DAPI (blue, nuclear staining)

Data (A-C) are presented as mean of indicated biological replicates ± SEM (n=x) and were normalized to respective DMSO control within each density and cell line. Statistics: two-tailed, unpaired T-test with Welch's correction (p-value: *<0.05, **<0.01, ***0.001, ****<0.0001, n.s. = not significant).

Fig EV2

A. Viability assay: treatment of HMLE-Twist1 and HMLE-Twist1-HRas with 0.3% DMSO or 30 nM RSL3 cells in density, n=2

B. Immunoblot: phosphorylated AKT at serine residue 473 (pAKT Ser473), total AKT 1 and 2 isoforms (pan AKT) and beta-actin protein expression in *PTEN*-wildtype (WT) and two *PTEN*-knockout clones (KO-1 and KO-2) of HMLE-Twist1-ER cells (without

Twist1-activation). Cells were grown in supplemented mammary epithelial growth medium (ctrl) or in basal DMEM/F-12 medium (starve). beta-actin serves as loading control. kDa = kilo Dalton

C. Viability assay: treatment of sorted, CD10-positive primary mammary epithelial cells of the basal lineage (B cells) of Donor with 0.1% DMSO or 100 nM RSL3 at ambient oxygen level (20%) or oxygen levels present in tissues (normoxia, 3%) in density, n=3

D. 3D-collagen gels: Bulk primary mammary epithelial cells were treated with 0.1% DMSO, 100 nM RSL3, 500 nM Lip1 or a combination of RSL3 and Lip1 for 7-10d prior quantification of arising colonies. Bright-field images of representative colonies and the mean of 3-4 technical replicates ± s.d. of one experiment performed are shown. Scale: 200 µm.

E. 3D-collagen gels: representative carmine stainings (left) with magnifications (right) showing colonies in black of HMLE single cell clone H5 with *GPX4*-knockout (KO) are shown. H5 was seeded at indicated densities in 3D collagen gels in medium containing 500 nM Lip1 (+Lip1), withdrawn of Lip1 either directly (-Lip1) or after 3d in initial +Lip1 culture (+/- Lip1) for 7-10 days, related to Fig 2F

Data (A,C) are presented as mean of indicated biological replicates ± SEM (n=x) and were normalized to respective DMSO control within each density and cell line. Statistics: two-tailed, unpaired T-test with Welch's correction (p-value: *<0.05, **<0.01, ***0.001, ****<0.0001, n.s. = not significant).

Figure 3: Cell density-dependent death induced by GPX4-inhibition is dependent on iron and oxidation of lipids, but independent of ACSL4.

A. Scheme showing regulators of ferroptosis and their inhibitors, GPX4: glutathione peroxidase 4, ACSL4: Acyl-CoA Synthetase Long Chain Family Member 4, ROSI: Rosiglitazone, LOX: lipoxygenase, PUFA: poly-unsaturated fatty acid, PE: phosphatidylethanolamine, -OOH: hydroperoxide, α-toc: α-tocopherol, DFO: Deferoxamine, CPX: Ciclopirox, Lip1: Liproxstatin1, Fer1: Ferrostatin1, ROS: reactive oxygen species.

B. Rescue-viability assay: treatment HMLE and HMLE-Twist1 cells with the indicated compounds as described in A alone or in a combination with 100 nM RSL3 at low density, mean of at least two biological replicates (n=2-5)

C. Immunoblot (top): ACSL4 and beta-actin (loading control) protein expression in Single Cell Clones (SCCs) of HMLE H5 *GPX4*-KO cells derived upon CRISPR/Cas9-mediated modification in the *ACSL4* locus. kDa = kilo Dalton. Viability assay (bottom): deprivation of 1 µM Lip1 in CRISPR/Cas9-derived SCCs with *ACSL4*-knockout (*ACSL4*-KO) or intact *ACSL4*-expression (*ACSL4*-WT) in density, n=3

D. Flow cytometry: C11-BODIPY staining of *GPX4*-knockout SCCs seeded at different densities in 1 µM Lip1 medium (+Lip1, blue) or in medium without Lip1 (−Lip1, orange). X-axis: log10 of C11 fluorescence, Y-axis: percentage of the maximum count, one representing experiment showing variation in fluorescence level is shown

E. Quantification of C11-fluoresence of HMLE and HMLE-Twist1 single cell clones (2 clones of H-SCCs and 3 clones of HT-SCCs, respectively) upon *GPX4*-knockout (−Lip1) normalized to respective +Lip1 control seeded and stained as described in Fig 3C. n=6

Data are presented as mean of indicated biological replicates ± SEM (n=x). Data was normalized to respective DMSO control (B) or to respective +Lip1 control (C, E) within

each seeding density and cell line. Statistics: two-tailed, unpaired T-test with Welch's correction (p-value: *<0.05, **<0.01, ***0.001, ****<0.0001, n.s. = not significant).

Figure 4: Proteomics reveal a density-dependent metabolic switch that sensitizes cells to ACSL4-independent ferroptosis

A. Venn diagram of proteomic data sets representing >1.5 fold upregulated proteins (p-value: <0.05) in density (left) and upon 5h 100 nM RSL3 treatment (right). The left circle shows common upregulated proteins in the lowest cell density compared to the highest cell density in both HMLE and HMLE-Twist1 cells. The right circle shows common upregulated proteins upon RSL3-treatment compared to non-RSL3 treated controls in both cell lines. The overlapping 119 proteins are upregulated both under low density conditions and upon RSL3 treatment. Interesting GO Terms of the overlapping proteins are listed.
B. Immunoblot: ATGL and beta-actin (loading control) protein expression in HMLE and HMLE-Twist1 cells seeded in density, kDa = kilo Dalton.
C. Flow cytometry: BODIPY493/503 and C11-BODIPY staining of HMLE and HMLE-Twist1 cells seeded at low (orange), intermediate (med, blue) and high (hi, grey) density. X-axis: log10 of respective fluorescence, Y-axis: percentage of the maximum count
D. Viability assay: treatment of HMLE and HMLE-Twist1 seeded at low density in 96-wells with 0.1% DMSO (-RSL3) or 100 nM RSL3 (+RSL3) only (ctrl, orange) or pre-treated for 24h with 20 µM Atglistatin (ATG, blue). ATG was present during DMSO/RSL3 treatment, n=4

E. RT-qPCR: CPT1A mRNA expression of HMLE and HMLE-Twist1 cells seeded in density. Mean of three technical replicates ± SEM of one representative experiment from two independent experiments performed are shown.

F. Flow cytometry: MitSox staining HMLE and HMLE-Twist1 cells seeded at low (orange), intermediate (med, blue) and high (hi, grey) density, X-axis: log10 of MitoSox fluorescence, Y-axis: percentage of the maximum count

G. Viability assay: treatment of HMLE and HMLE-Twist1 seeded at low density with 0.1% DMSO (-RSL3) or 100 nM RSL3 (+RSL3) only (ctrl, orange) or in presence of 100 µM Etomoxir (ETX, blue), n=4

H. Flow cytometry: BODIPY493/503 and C11-BODIPY staining of HMLE and HMLE-Twist1 cells seeded at low (orange), intermediate (med, blue) and high (hi, grey) density treated without (ctrl) or for 24h with 100 µM oleic acid (OA). X-axis: log10 of respective fluorescence, Y-axis: percentage of the maximum count

I. Viability assay: treatment of HMLE and HMLE-Twist1 seeded at indicated densities with 100 nM RSL3 (+RSL3) only (ctrl, orange) or pre-treated for 24h with 100 µM oleic acid (OA, blue). OA was present during DMSO/RSL3 treatment, n=3

Data (D,G,I) are presented as mean of indicated biological replicates ± SEM (n=x) and were normalized to respective DMSO control within each seeding density and cell ine. Statistics: two-tailed, unpaired T-test with Welch's correction (p-value: *<0.05, **<0.01, ***0.001, ****<0.0001, n.s. = not significant). Data (C,F,H) show one representative experiment from two (H), three (D) or four (F) independent experiments.

Figure EV3: ATGL regulation in cell-density contributes to density-dependent cell death

A. GO-term analyses: top 10, significantly enriched terms (biological processes) of upregulated proteins (119) in density and upon RSL3 treatment, related to Fig 4A
B. Viability assay: *GPX4*-knockout clones HMLE H5 and HMLE-Twist1 HT1 were seeded at indicated density in medium containing 1 µM Lip1 or without –Lip1 (ctrl, orange) or in addition treated with 20 µM Atglistatin (ATG, blue). Cells were pre-treated for 24h with ATG prior viability assay, n=3
C. RT-qPCR: ACAA2 mRNA expression of HMLE and HMLE-Twist1 cells seeded in density. Mean of three technical replicates ± SEM of one representative experiment from two independent experiments performed are shown.
D. Viability assay: *GPX4*-knockout clones HMLE H5 and HMLE-Twist1 HT1 were seeded at indicated density in presence of 1 µM Lip1 or without –Lip1 (ctrl, orange) or in addition treated with 100 µM Etomoxir (ETX, blue), n=3
E. Viability assay: treatment of HMLE and HMLE-Twist1 seeded at indicated densities with 0.1% DMSO only (ctrl, orange) or pre-treated for 24h with 100 µM oleic acid (OA, blue). OA was present during DMSO treatment, n=3, Figure relates to 4I

Data (B,D,E) are presented as mean of indicated biological replicates ± SEM (n=x) and were normalized to respective DMSO control within each seeding density and cell line. Statistics: two-tailed, unpaired T-test with Welch's correction (p-value: *<0.05, **<0.01, ***0.001, ****<0.0001, n.s. = not significant).

Figure 1

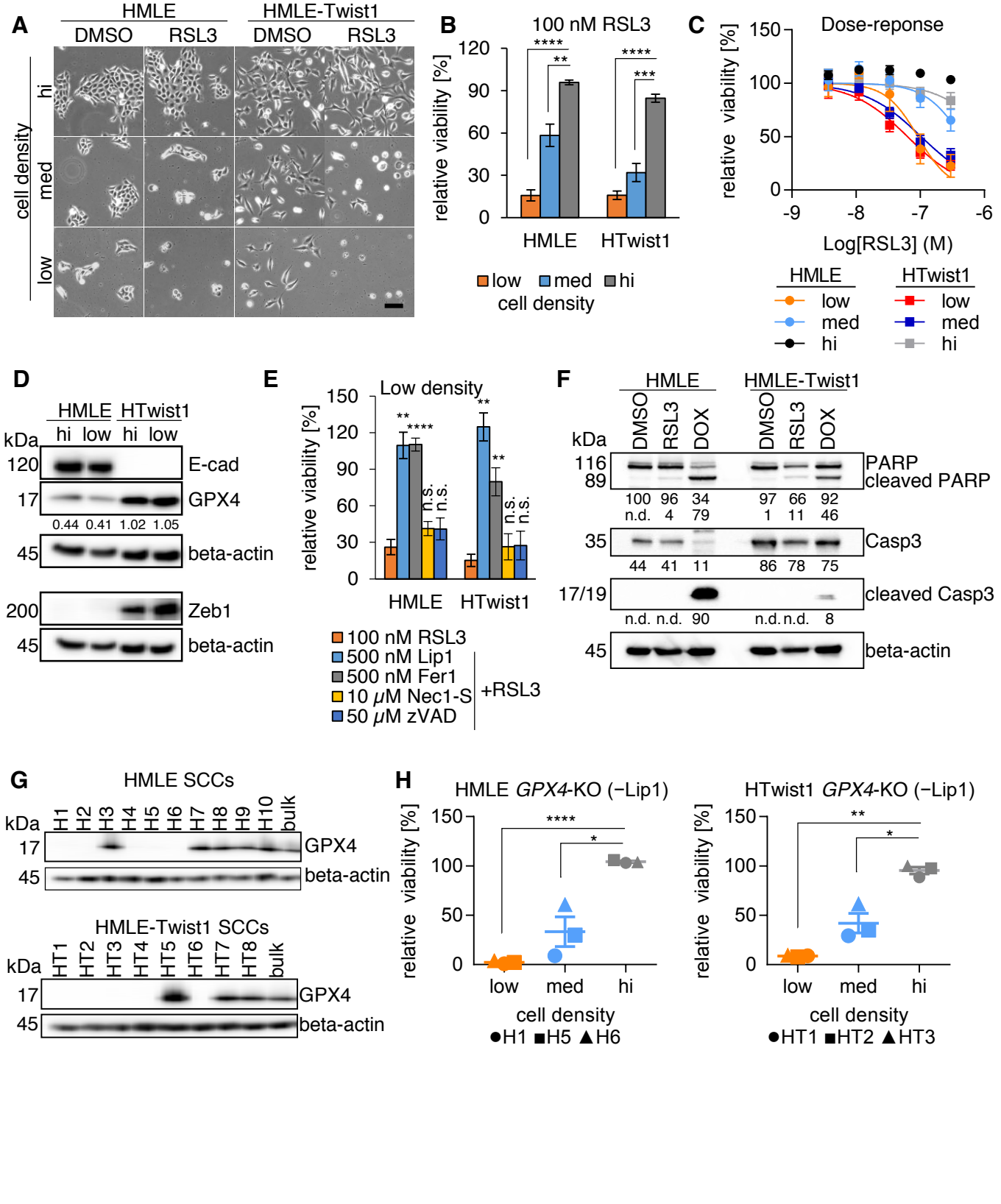
A
HMLE
HMLE-Twist1
DMSO
RSL3
DMSO
RSL3
cell density
hi
med
low
B
100 nM RSL3
relative viability [%]
HMLE
HTwist1
low
med
hi
cell density
C
Dose-reponse
relative viability [%]
Log[RSL3] (M)
HMLE
low
med
hi
HTwist1
low
med
hi
D
HMLE
HTwist1
kDa
hi
low
hi
low
120
E-cad
17
GPX4
0.44 0.41 1.02 1.05
45
beta-actin
200
Zeb1
45
beta-actin
E
Low density
relative viability [%]
HMLE
HTwist1
100 nM RSL3
500 nM Lip1
500 nM Fer1
10 μM Nec1-S
50 μM zVAD
+RSL3
F
HMLE
HMLE-Twist1
kDa
DMSO
RSL3
DOX
DMSO
RSL3
DOX
116
89
PARP
cleaved PARP
100 96 34 97 66 92
n.d. 4 79 1 11 46
35
Casp3
44 41 11 86 78 75
17/19
cleaved Casp3
n.d. n.d. 90 n.d. n.d. 8
45
beta-actin
G
HMLE SCCs
kDa
H1 H2 H3 H4 H5 H6 H7 H8 H9 H10 bulk
17
GPX4
45
beta-actin
HMLE-Twist1 SCCs
kDa
HT1 HT2 HT3 HT4 HT5 HT6 HT7 HT8 bulk
17
GPX4
45
beta-actin
H
HMLE GPX4-KO (−Lip1)
relative viability [%]
low
med
hi
cell density
●H1 ■H5 ▲H6
HTwist1 GPX4-KO (−Lip1)
relative viability [%]
low
med
hi
cell density
●HT1 ■HT2 ▲HT3

Figure 2

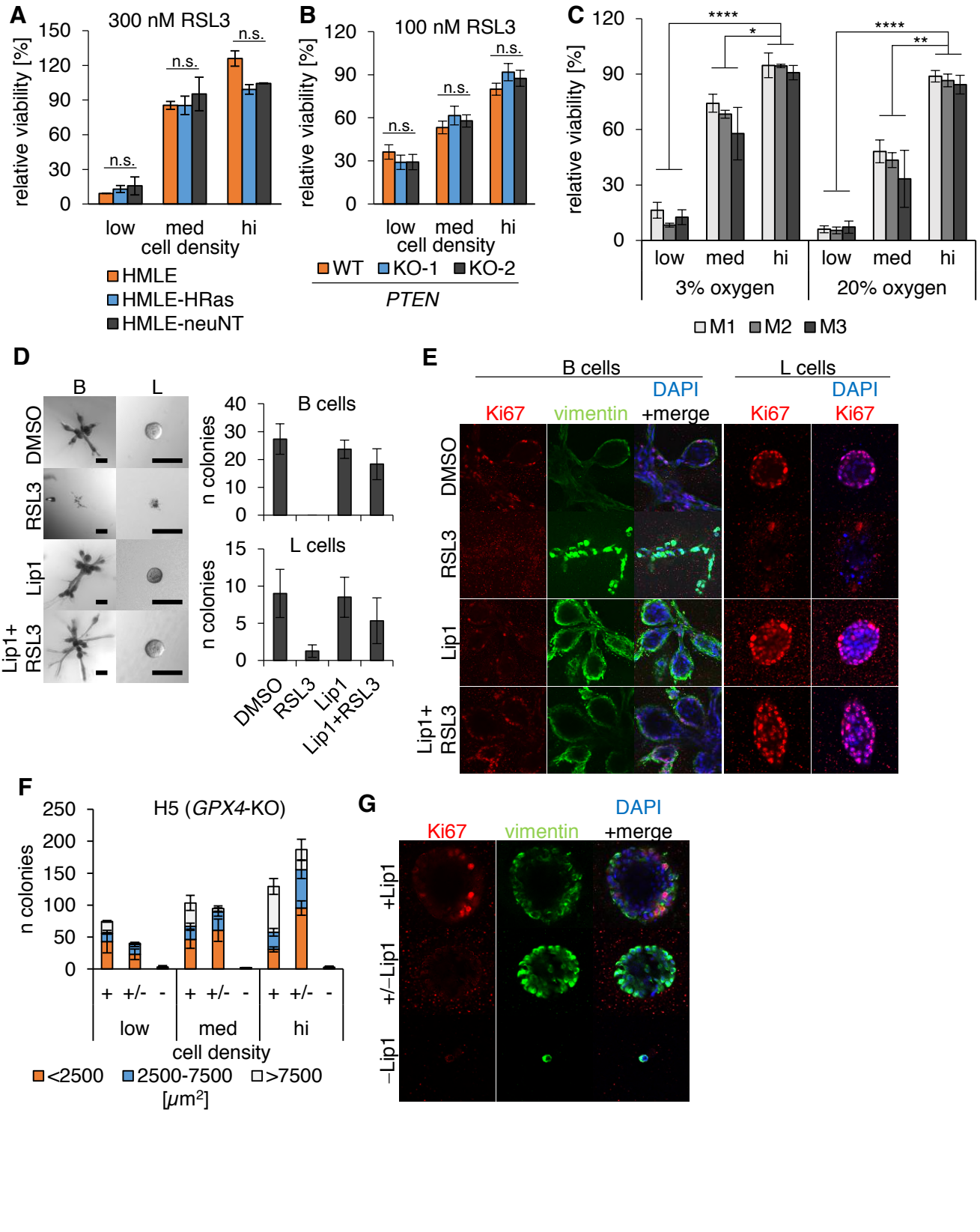
A
300 nM RSL3
relative viability [%]
n.s.
low med hi
cell density
HMLE
HMLE-HRas
HMLE-neuNT
B
100 nM RSL3
WT KO-1 KO-2
PTEN
C
****
*
**
low med hi
3% oxygen
20% oxygen
M1 M2 M3
D
B L
DMSO
RSL3
Lip1
Lip1+ RSL3
B cells
L cells
n colonies
DMSO
RSL3
Lip1
Lip1+RSL3
E
B cells
L cells
DAPI
Ki67
vimentin
+merge
F
H5 (GPX4-KO)
n colonies
low med hi
cell density
<2500
2500-7500
>7500
[μm²]
G
Ki67
vimentin
DAPI
+merge
+Lip1
+/–Lip1
–Lip1

Figure 3

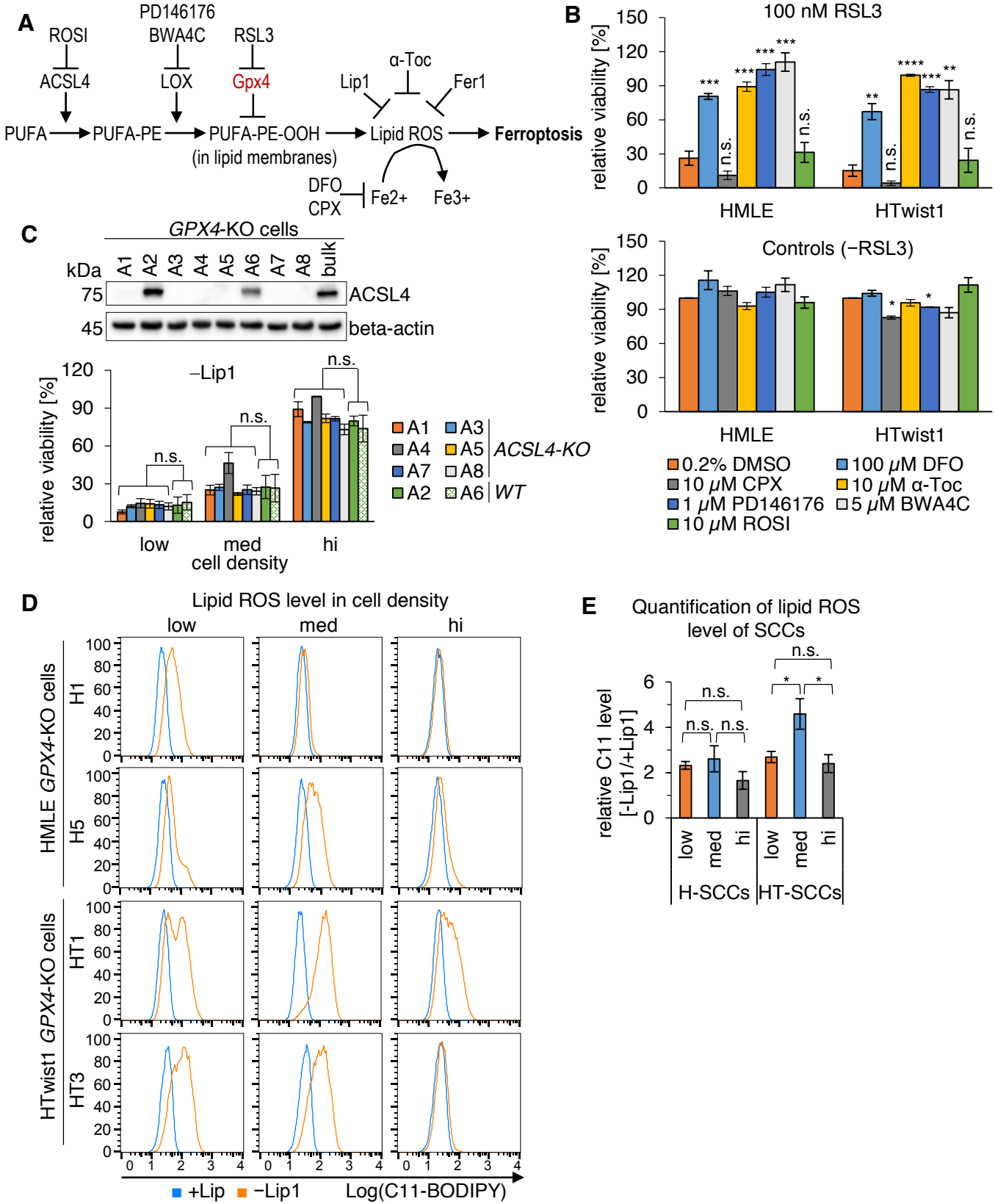
A
ROSI
ACSL4
PD146176
BWA4C
LOX
RSL3
Gpx4
α-Toc
Lip1
Fer1
PUFA
PUFA-PE
PUFA-PE-OOH
(in lipid membranes)
Lipid ROS
Ferroptosis
DFO
CPX
Fe2+
Fe3+
B
100 nM RSL3
relative viability [%]
HMLE
HTwist1
Controls (−RSL3)
0.2% DMSO
100 μM DFO
10 μM CPX
10 μM α-Toc
1 μM PD146176
5 μM BWA4C
10 μM ROSI
C
GPX4-KO cells
kDa
A1 A2 A3 A4 A5 A6 A7 A8 bulk
75
ACSL4
45
beta-actin
−Lip1
relative viability [%]
n.s.
low
med
hi
cell density
A1 A3 A4 A5 A7 A8 ACSL4-KO
A2 A6 WT
D
Lipid ROS level in cell density
low
med
hi
HMLE GPX4-KO cells
H1
H5
HTwist1 GPX4-KO cells
HT1
HT3
+Lip
−Lip1
Log(C11-BODIPY)
E
Quantification of lipid ROS level of SCCs
relative C11 level [-Lip1/+Lip1]
low
med
hi
H-SCCs
HT-SCCs

Figure 4

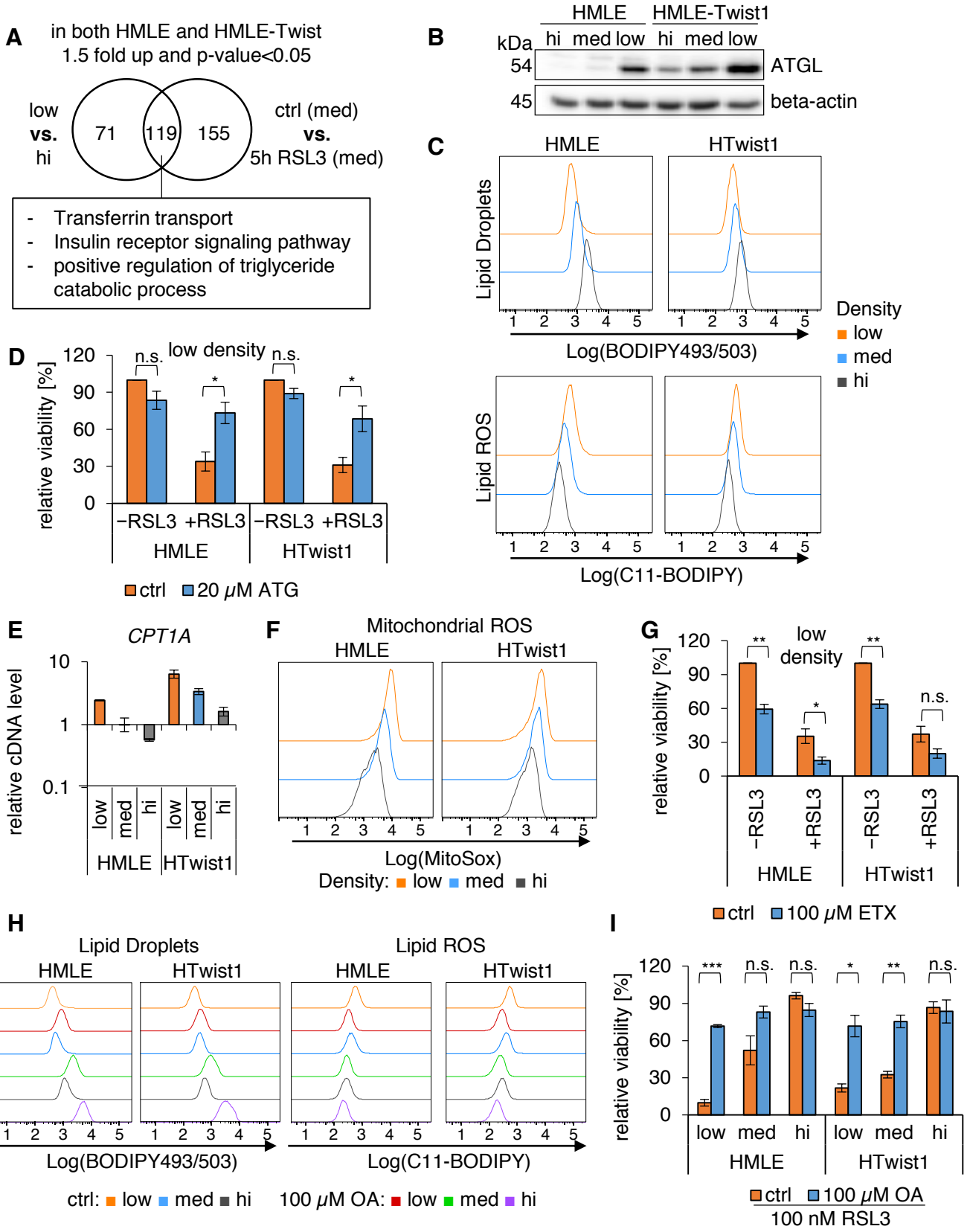
A
in both HMLE and HMLE-Twist
1.5 fold up and p-value<0.05
low vs. hi
71
119
155
ctrl (med) vs. 5h RSL3 (med)
- Transferrin transport
- Insulin receptor signaling pathway
- positive regulation of triglyceride catabolic process
B
HMLE
HMLE-Twist1
kDa
hi med low hi med low
54
ATGL
45
beta-actin
C
HMLE
HTwist1
Lipid Droplets
Log(BODIPY493/503)
Lipid ROS
Log(C11-BODIPY)
Density
low
med
hi
D
relative viability [%]
low density
n.s.
*
−RSL3 +RSL3 −RSL3 +RSL3
HMLE
HTwist1
ctrl
20 μM ATG
E
CPT1A
relative cDNA level
low med hi low med hi
HMLE
HTwist1
F
Mitochondrial ROS
HMLE
HTwist1
Log(MitoSox)
Density: low med hi
G
relative viability [%]
low density
**
*
n.s.
−RSL3 +RSL3 −RSL3 +RSL3
HMLE
HTwist1
ctrl
100 μM ETX
H
Lipid Droplets
Lipid ROS
HMLE
HTwist1
Log(BODIPY493/503)
Log(C11-BODIPY)
ctrl: low med hi
100 μM OA: low med hi
I
relative viability [%]
***
n.s.
*
**
low med hi low med hi
HMLE
HTwist1
ctrl
100 μM OA
100 nM RSL3

Figure EV1

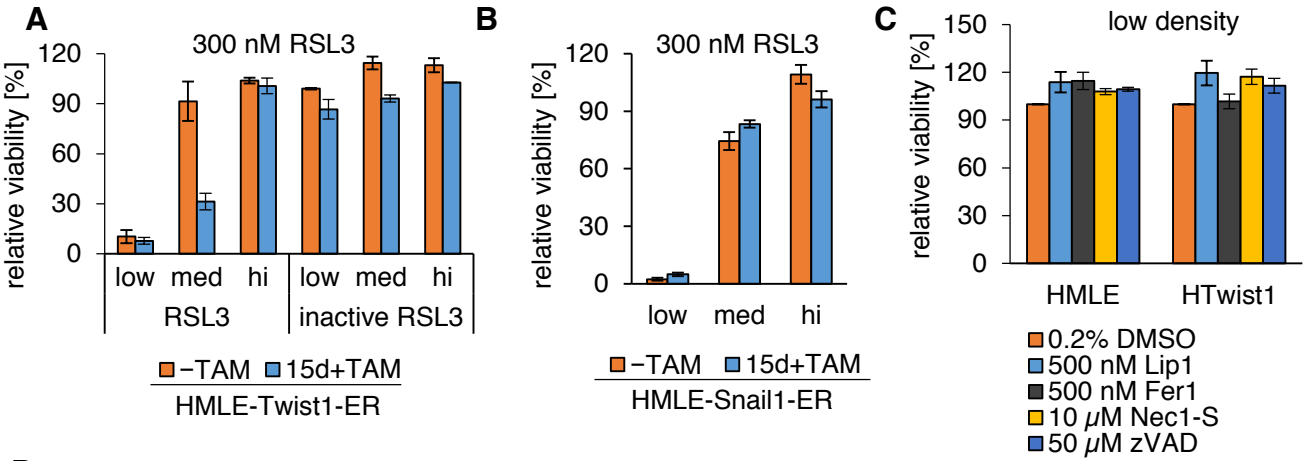
A
300 nM RSL3
relative viability [%]
120
90
60
30
0
low med hi low med hi
RSL3
inactive RSL3
−TAM 15d+TAM
HMLE-Twist1-ER
B
300 nM RSL3
relative viability [%]
low med hi
−TAM 15d+TAM
HMLE-Snail1-ER
C
low density
relative viability [%]
150
120
90
60
30
0
HMLE HTwist1
0.2% DMSO
500 nM Lip1
500 nM Fer1
10 μM Nec1-S
50 μM zVAD

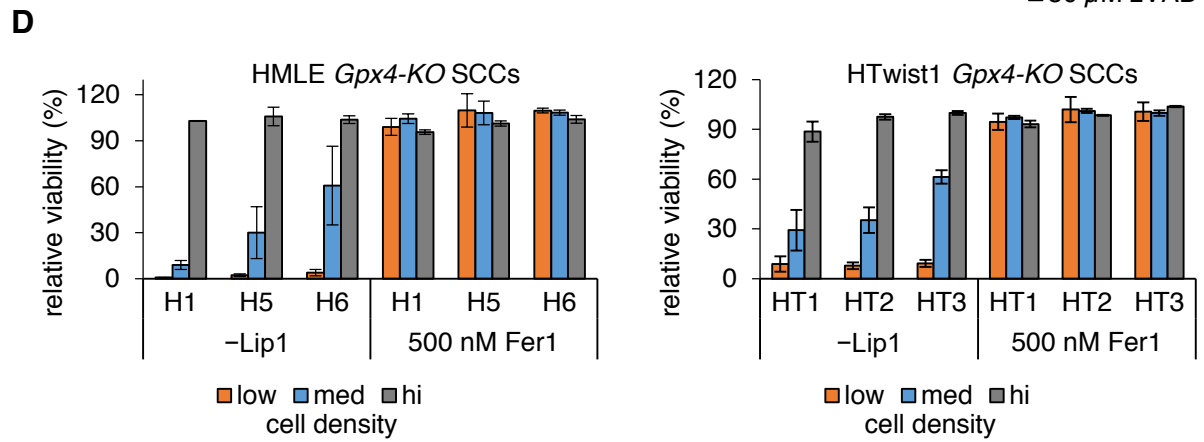
D
HMLE Gpx4-KO SCCs
relative viability (%)
120
90
60
30
0
H1 H5 H6 H1 H5 H6
−Lip1
500 nM Fer1
low med hi
cell density
HTwist1 Gpx4-KO SCCs
relative viability (%)
HT1 HT2 HT3 HT1 HT2 HT3
−Lip1
500 nM Fer1
low med hi
cell density

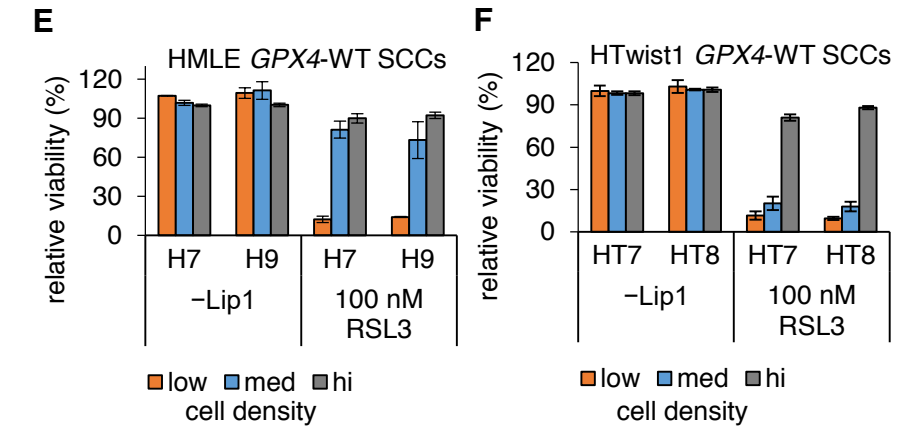
E
HMLE GPX4-WT SCCs
relative viability (%)
120
90
60
30
0
H7 H9 H7 H9
−Lip1
100 nM RSL3
low med hi
cell density
F
HTwist1 GPX4-WT SCCs
relative viability (%)
HT7 HT8 HT7 HT8
−Lip1
100 nM RSL3
low med hi
cell density

Figure EV2

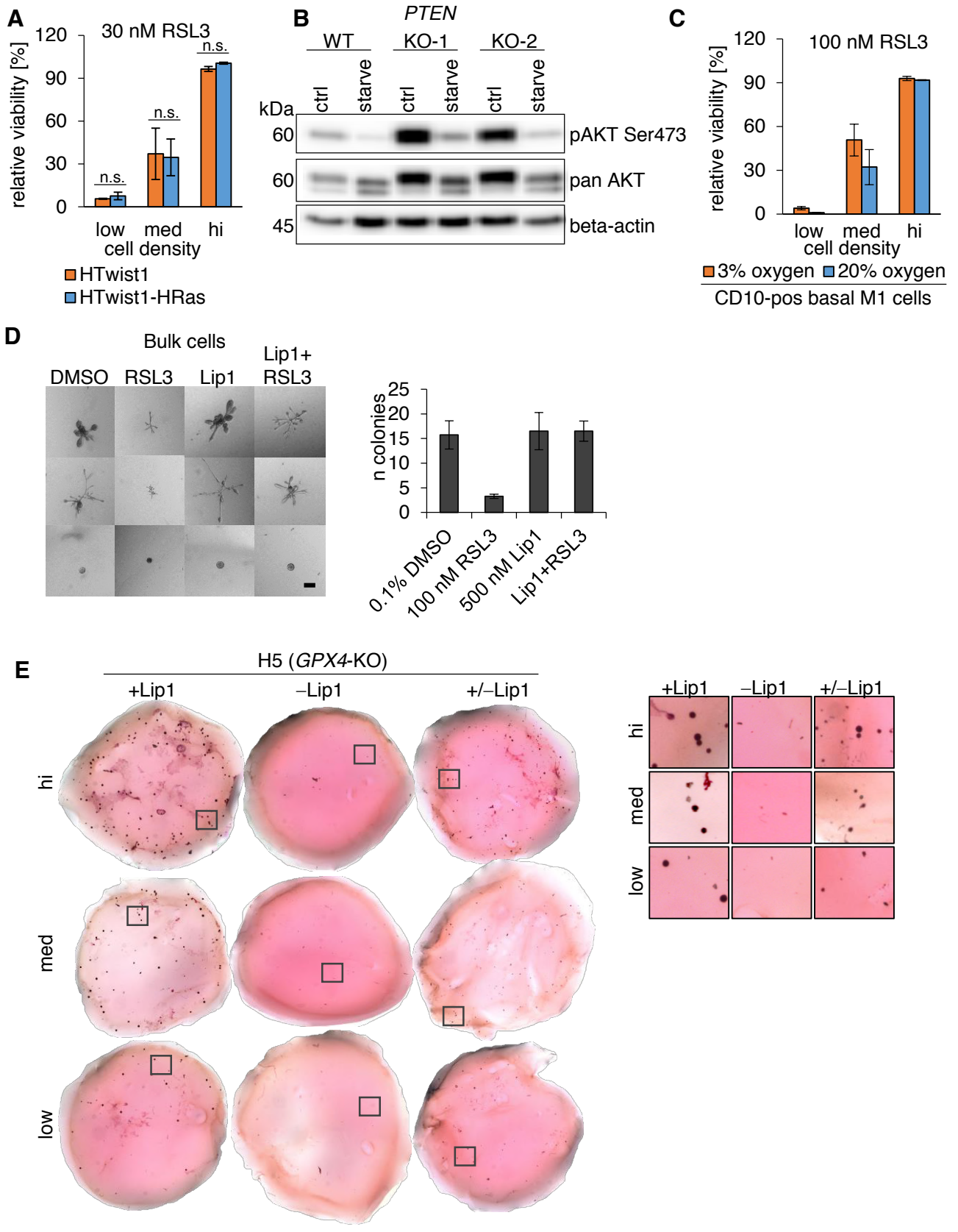
A
30 nM RSL3
relative viability [%]
120
90
60
30
0
n.s.
n.s.
n.s.
low
med
hi
cell density
HTwist1
HTwist1-HRas
B
PTEN
WT
KO-1
KO-2
ctrl
starve
kDa
60
60
45
pAKT Ser473
pan AKT
beta-actin
C
100 nM RSL3
relative viability [%]
120
90
60
30
0
low
med
hi
cell density
3% oxygen
20% oxygen
CD10-pos basal M1 cells
D
Bulk cells
DMSO
RSL3
Lip1
Lip1+ RSL3
n colonies
25
20
15
10
5
0
0.1% DMSO
100 nM RSL3
500 nM Lip1
Lip1+RSL3
E
H5 (GPX4-KO)
+Lip1
–Lip1
+/–Lip1
hi
med
low
+Lip1
–Lip1
+/–Lip1
hi
med
low

Figure EV3

A

Term	p-Value	Gene names
transferrin transport (GO:0033572)	3.17E-09	ATP6V1A, ATP6V1B1, ATP6V1B2, ATP6V1D, ATP6V1E1, ATP6V1E2, ATP6V1H, RAB11B
regulation of macroautophagy (GO:0016241)	1.72E-08	ATP6V1A, ATP6V1B1, ATP6V1B2, ATP6V1D, ATP6V1E1, ATP6V1E2, ATP6V1H, UCHL1
phagosome acidification (GO:0090383)	2.26E-08	ATP6V1A, ATP6V1B1, ATP6V1B2, ATP6V1D, ATP6V1E1, ATP6V1E2, ATP6V1H
ATP hydrolysis coupled proton transport (GO:0015991)	2.30E-06	ATP6V1A, ATP6V1B1, ATP6V1B2, ATP6V1E1, ATP6V1E2, ATP6V1H
insulin receptor signaling pathway (GO:0008286)	1.48E-05	ATP6V1A, ATP6V1B1, ATP6V1B2, ATP6V1D, ATP6V1E1, ATP6V1E2, ATP6V1H
proton transport (GO:0015992)	3.37E-04	ATP6V1A, ATP6V1B1, ATP6V1B2, ATP6V1D, ATP6V1E1
positive regulation of exocytosis (GO:0045921)	3.71E-04	RAB3A, CADPS2, FGB, FGG
synaptic vesicle exocytosis (GO:0016079)	4.27E-04	RAB3A, CADPS2, CADPS, VAMP2
ion transmembrane transport (GO:0034220)	5.75E-04	ATP6V1A, ATP6V1B1, ATP6V1B2, ATP6V1D, ATP6V1E1, ATP6V1E2, ATP6V1H, GRIK3
positive regulation of triglyceride catabolic process (GO:0010898)	1.25E-03	ABHD5, APOA4, **PNPLA2**

B

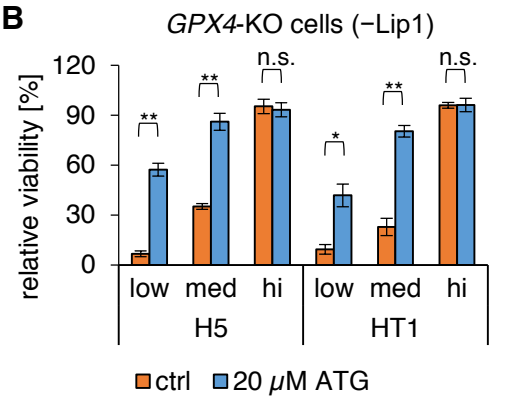

C

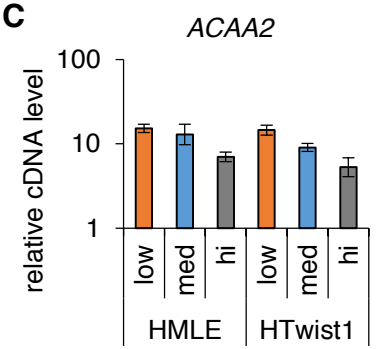

D

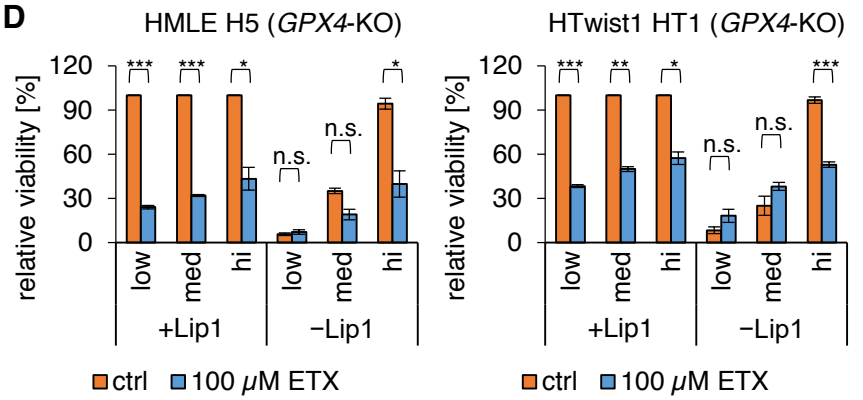

E